

# NASA Technical Memorandum 104543

**ORIGINAL CONTAINS  
COLOR ILLUSTRATIONS**

## **Geoid Undulations and Gravity Anomalies Over the Aral Sea, the Black Sea and the Caspian Sea From a Combined GEOS-3/SEASAT/ GEOSAT Altimeter Data Set**

**Andrew Y. Au and Richard D. Brown**  
*ST Systems Corporation*  
*Lanham, Maryland*

**Jean E. Welker**  
*Goddard Space Flight Center*  
*Greenbelt, Maryland*

**NASA**

National Aeronautics and  
Space Administration

**Goddard Space Flight Center**  
Greenbelt, MD

1991

## **PREFACE**

Satellite-based altimetric data taken by GEOS-3, SEASAT and GEOSAT over the Aral Sea, the Black Sea and the Caspian Sea are analyzed and a least-squares collocation technique is used to predict the geoid undulations on a  $0.25^\circ \times 0.25^\circ$  grid and to transform these geoid undulations to free air gravity anomalies. Rapp's 180 X 180 geopotential model is used as the reference surface for the collocation procedure. The result of geoid-to-gravity transformation is, however, sensitive to the information content of the reference geopotential model used. For example, considerable detailed surface gravity data have been incorporated into the reference model over the Black Sea, resulting in a reference model with significant information content at short wavelengths. Thus estimation of short-wavelength gravity anomalies from gridded geoid heights is generally reliable over regions such as the Black Sea, using the conventional collocation technique with local empirical covariance functions. Over regions, such as the Caspian Sea, where detailed surface data are generally not incorporated into the reference model, unconventional techniques are needed to obtain reliable gravity anomalies. Based on the predicted gravity anomalies over these inland seas, speculative tectonic structures are identified and geophysical processes are inferred.

## CONTENTS

LIST OF FIGURES	v
I. INTRODUCTION	1
II. ALTIMETER DATA	3
Crossover Adjustments	3
III. APPLICATION OF COLLOCATION TECHNIQUE	11
Collocation Gridding of Geoid Undulations	11
Estimation of Gravity Anomalies	23
IV. ROBUSTNESS TEST FOR THE GEOID-TO-GRAVITY TRANSFORMATION	27
V. GEOPHYSICAL INFERENCES	44
REFERENCES	46

## List of Figures

- Figure 1. GEOS-3, SEASAT and GEOSAT altimeter data distribution over the Aral Sea.
- Figure 2. GEOS-3, SEASAT and GEOSAT altimeter data distribution over the Black Sea.
- Figure 3. GEOS-3, SEASAT and GEOSAT altimeter data distribution over the Caspian Sea.
- Figure 4. Sample adjusted altimeter elevation profiles of the Black Sea. Profile of the reference pass. Dashed line is Rapp's 180 X 180 reference geoid.
- Figure 5. Sample adjusted altimeter elevation profiles of the Caspian Sea. Profile of the reference pass. Dashed line is Rapp's 180 X 180 reference geoid.
- Figure 6. Sample adjusted altimeter elevation profiles of the Aral Sea. Profile of the reference pass. Dashed line is Rapp's 180 X 180 reference geoid.
- Figure 7. Normalized local residual empirical covariance functions of the Aral Sea. The normalization coefficients for:
- 1) geoid-geoid (solid line) is  $3.27 \text{ m}^2$ ,
  - 2) geoid-gravity (dashed line) is  $23.48 \text{ m-mgal}$ , and
  - 3) gravity-gravity (dotted line) is  $826.17 (\text{mgal})^2$ .
- Figure 8. Normalized local residual empirical covariance functions of the Black Sea. The normalization coefficients for:
- 1) geoid-geoid (solid line) is  $1.61 \text{ m}^2$ ,
  - 2) geoid-gravity (dashed line) is  $9.76 \text{ m-mgal}$ , and
  - 3) gravity-gravity (dotted line) is  $173.2 (\text{mgal})^2$ .
- Figure 9. Normalized local residual empirical covariance functions of the Caspian Sea. The normalization coefficients for:
- 1) geoid-geoid (solid line) is  $8.86 \text{ m}^2$ ,
  - 2) geoid-gravity (dashed line) is  $44.11 \text{ m-mgal}$ , and
  - 3) gravity-gravity (dotted line) is  $345.8 (\text{mgal})^2$ .
- Figure 10. A contour map of the collocation geoid undulations of the Aral Sea (m above mean sea level) gridded with local empirical geoid-geoid covariance function.
- Figure 11. A contour map of the collocation geoid undulations of the Black Sea (m above mean sea level) gridded with local empirical geoid-geoid covariance function.
- Figure 12. A contour map of the collocation geoid undulations of the Caspian Sea (m above mean sea level) gridded with local empirical geoid-geoid covariance function.

Figure 13. A contour map of Rapp's 180 X 180 reference geoid undulations (m above mean sea level) of the Aral Sea.

Figure 14. A contour map of Rapp's 180 X 180 reference geoid undulations (m above mean sea level) of the Black Sea.

Figure 15. A contour map of Rapp's 180 X 180 reference geoid undulations (m above mean sea level) of the Caspian Sea.

Figure 16. Normalized Rapp's 180 X 180 global covariance functions. The normalization coefficients for:

- 1) geoid-geoid (solid line) is  $1.13 \text{ m}^2$ ,
- 2) geoid-gravity (dashed line) is  $7.26 \text{ m-mgal}$ , and
- 3) gravity-gravity (dotted line) is  $98.36 \text{ (mgal)}^2$ .

Figure 17. Normalized Jordan's theoretical covariance functions of the Caspian Sea. The normalization coefficients for:

- 1) geoid-geoid (solid line) is  $8.86 \text{ m}^2$ ,
- 2) geoid-gravity (dashed line) is  $45.20 \text{ m-mgal}$ , and
- 3) gravity-gravity (dotted line) is  $345.8 \text{ (mgal)}^2$ .

Figure 18. A contour map of estimated gravity anomalies (mgal) of the Aral Sea predicted with local empirical covariance functions.

Figure 19. A contour map of estimated gravity anomalies (mgal) of the Black Sea predicted with local empirical covariance functions.

Figure 20. A contour map of estimated gravity anomalies (mgal) of the Caspian Sea predicted with hybrid local empirical covariance functions.

Figure 21. A contour map of Rapp's 180 X 180 reference gravity anomalies (mgal) of the Aral Sea.

Figure 22. A contour map of Rapp's 180 X 180 reference gravity anomalies (mgal) of the Black Sea.

Figure 23. A contour map of Rapp's 180 X 180 reference gravity anomalies (mgal) of the Caspian Sea.

Figure 24. A contour map of Rapp's 36 X 36 reference geoid undulations (m above mean sea level) of the Black Sea.

Figure 25. A contour map of Rapp's 36 X 36 reference gravity anomalies (mgal) of the Black Sea.

Figure 26. A contour map of estimated gravity anomalies (mgal) of the Black Sea based on Rapp's 36 X 36 reference geopotential model.

**Figure 27.** A contour map of the difference between estimated gravity anomalies (mgal) of the Black Sea using Rapp's 36 X 36 and 180 X 180 reference geopotential models.

**Figure 28.** A contour map of estimated gravity anomalies (mgal) of the Black Sea based on Rapp's 180 X 180 reference geopotential model and the self-consistent iterative approach. Rapp's 300 x 300 model geoid undulations are used as input data. This is a test of the iterative approach.

**Figure 29.** A contour map of estimated gravity anomalies (mgal) of the Black Sea based on Rapp's 36 X 36 reference geopotential model and the self-consistent iterative approach. Rapp's 300 x 300 model geoid undulations are used as input data. This is a test of the iterative approach.

**Figure 30.** A contour map of Rapp's 300 X 300 reference geoid undulations (m above mean sea level) of the Black Sea.

**Figure 31.** A contour map of Rapp's 300 X 300 reference gravity anomalies (mgal) of the Black Sea.

**Plate 1.** A contour map of Rapp's 180 X 180 reference gravity anomalies (mgal) of the inland seas region.

**Plate 2.** A contour map of predicted gravity anomalies (mgal) of the inland seas region. (a) Continuous suture running from the Crimea, along the spine of the Greater Caucasus, through the Aspheron peninsula, across the southern Caspian, and into the Kopet mountains; (b) Band of positive anomalies in alignment with the Dnieper-Donetsk aulacogen and the South Mangyshlak-Ust-Yurt ridge and basin; (c) Tethyan geosyncline tracing southward, running across the northern reach of the Black Sea, into the northern part of the Caspian Sea, and then going northward; (d) The west Black Sea depression; (e) The east Black Sea depression; (f) The Andrusov Swell; (g) The Arkhangelsky Swell; (h) The Shatsky Swell; (i) The Danube delta; (j) The Volga delta; (k) The Ural delta; (l) The Syr-Dar'ya delta and (m) The Amu-Dar'ya delta.

INTERNATIONAL BANKING CORPORATION

## INTRODUCTION

This paper documents and summarizes the processing of satellite altimeter data over inland seas (the Aral, the Black, and the Caspian Seas) for recovery of area-mean gravity information. Based on predicted gravity anomalies over the inland seas, geophysical inferences on the tectonic features in this region are made.

Gravity information in this area of the world is not readily available, so the possibility of obtaining it from the processing of altimeter observations is attractive. The mean surface level of the seas approximates an equipotential surface. Therefore, information about the gravity potential and gravity can be obtained from altimetric measurement of the relative shape of this surface.

Local gravity anomalies recovered from satellite-based altimeter data have been performed by Knudsen (1987, 1988) in  $2^\circ \times 2^\circ$  areas in North Atlantic ocean, by Mazzega and Houry (1989) for the Mediterranean and the Black Seas, by Au *et al.* (1989a) over the Black and the Caspian Seas, and by Au *et al.* (1990) over the Aral Sea. The local covariance functions used in the works of Knudsen (1987, 1988) and Mazzega and Houry (1989) are determined from spectral analysis of global models, whereas those in our previous work are determined by numerical convolution. Although these two processes are ideally equivalent given complete global data, the convolution method ensures the integration of available local information into the covariance functions.

The basic approach used by this study is:

1. Edit geoid height data to remove overland data;
2. Evaluate geoid height differences at crossover points;
3. Remove orbit errors from geoid heights using crossover differences;
4. Grid geoid height data at  $0.25^\circ \times 0.25^\circ$  intervals;
5. Estimate  $0.25^\circ \times 0.25^\circ$  gravity anomalies from gridded geoid heights using the collocation technique.

The need for step 1 is obvious. Steps 2 and 3 are necessary because satellite altimeter measurements cannot yield accurate sea-surface heights unless variations in satellite heights due to orbit errors are removed and all passes are reduced to a common reference. If the sea-surface elevation at a given location is constant over the time span of the altimeter data used, any difference in surface height between two crossing altimeter passes is due to orbit differences. Differences in sea-surface elevation up to about 50 cm could be due to tides, especially solid earth tides, whose amplitude is about 25 cm. Because the orbit differences are nearly constant for the short arcs over the inland seas, removal of a constant bias from each pass based on crossover differences should effectively rectify orbit differences. In this process, one pass is held fixed, whereas all others are adjusted relative to it. The height of the reference pass, then, is adjusted to agree with the mean sea-surface elevation of the sea. Area-mean surface-height values are determined and reduced to the reference geoid in step 4. In step 5 these area-mean geoid heights are processed and area-mean gravity anomaly values are predicted using a linear least-squares estimation technique, called collocation, formulated by Moritz (1978). The



collocation technique is essentially a differential operation transforming geopotential information to its first derivative, gravity. Knowledge of the statistical correlation between area-mean geoid heights and gravity anomalies is required in the geoid-to-gravity transformation.

Of the three sources of altimeter data used, GEOS-3 altimeter data is of lowest quality (standard deviation between 25 and 50 cm, depending on operating mode; see Wagner, 1979) and is of lower quality than that of SEASAT (standard deviation from 6 to 10 cm; see Townsend, 1980), primarily because SEASAT used an advanced radar altimeter design. SEASAT data, in turn, is of lower quality than that of GEOSAT (standard deviation less than 5 cm; see Cheney *et al.*, 1989). The two GEOS-3 altimeter operating modes, intensive and global, are differentiated primarily by data rate, which explains the corresponding difference in quality. The GEOS-3 mission collected data between 1975 and 1978 over latitudes up to 65 degrees, whereas SEASAT collected data only during 100 days in 1978 over latitudes up to 72 degrees. The GEOSAT, since October 1986, has repeated the same ground track of the ill-fated SEASAT in a 17-day Exact Repeat Mission (ERM).

In the next section, steps 1 to 3 are discussed in detail. Results of the application of least-squares collocation technique to both geoid gridding and gravity prediction are presented in section III. A discussion on the robustness of the algorithm used in the gravity prediction is given in Section IV. In Section V geophysical inferences on the inland sea region are attempted based on the predicted gravity results. Detail documentation of the work over the Black and the Caspian Seas using GOES-3 and SEASAT altimeter data can be found in Au *et al.* (1989a), whereas detailed analysis of gravity prediction for the Aral Sea using altimeter data can be found in Au *et al.* (1990). The program software package used in the altimetry analysis is given in Au *et al.* (1989b).

## II. ALTIMETER DATA

Altimeter data over the inland seas, were obtained from NASA/GSFC in the GEODYN program format. All available GEOS-3 and SEASAT data are used in the analysis. The inclusion of GEOSAT Extended Repeat Mission (ERM) data in the analysis over the Black Sea and the Caspian Sea does not substantially improve the geometry of the data coverage over the two areas, because the location of the GEOSAT and the SEASAT subtracks are nearly coincident. Therefore, from each set of the GEOSAT ERM repeat passes over the two seas only one representative pass has been used. On the other hand, due to the scarcity of data over the Aral Sea, as many GEOSAT repeat passes as possible are considered in the data analysis.

The geodetic positions of the altimeter ground track data of the three satellites over the Aral, the Black and the Caspian Sea are shown in Figures 1, 2 and 3, respectively. There are 83 GEOS-3, 62 SEASAT and 20 GEOSAT passes over the Black Sea written in 10146 data records. Over the Caspian Sea there are 71 GEOS-3, 23 SEASAT and 15 GEOSAT passes written in 21484 data records. Over the Aral Sea there are only 7 GEOS-3, 16 SEASAT, but 151 GEOSAT passes written in 3037 data records. Visual examination of these surface elevation profiles over the Black and Caspian Seas suggests that the data are relatively noiseless, except for a few occurrences of data spikes and data gaps. In subsequent data processing, data spikes were eliminated by removing data points that deviate from adjacent values by more than an *a priori* assignment, which is 2 m for the Black Sea and 10 m for the Caspian Sea. An in-depth description of the data-cleanup process for GOES-3 and SEASAT over the Black Sea and the Caspian can be found in Au *et al.* (1989a).

It can be seen, however, from Figure 1 that the data coverage over the Aral Sea is incomplete and inhomogeneous, with major data gaps in the northwestern and southeastern regions. The quality of the data over the Aral Sea is also disappointing, with large number of data spikes, especially at the beginning and end of each ground track profile. Because it is difficult to distinguish signal from noise in an unadjusted satellite pass, over-enthusiastic data-cleaning will result in unnecessary decimation of the already small data set. Data spikes were, therefore, not edited out prior to satellite pass crossover adjustment. However, crossovers in the vicinity of data spikes were excluded from crossover adjustment. Questionable data records after crossover adjustment were again examined to determine if they are a consequence of loss-of-phase-lock, especially if they are at the beginning or at the end of a pass. Noisy data records, then, were removed from subsequent analysis. An in-depth description of the data-cleanup process for GOES-3, SEASAT and GEOSAT over the Aral Sea can be found in Au *et al.* (1990).

### Crossover Adjustments

The major error source in altimetric geoid undulations is the uncertainty in the radial component of the satellite trajectory. This uncertainty is manifest in the misclosure of surface elevation at ground-track intersections (crossovers) between passes. For the short arcs of data considered here, the orbit error can be modeled as a bias applied to all the data of a given pass. The optimum biases are such that crossover differences are

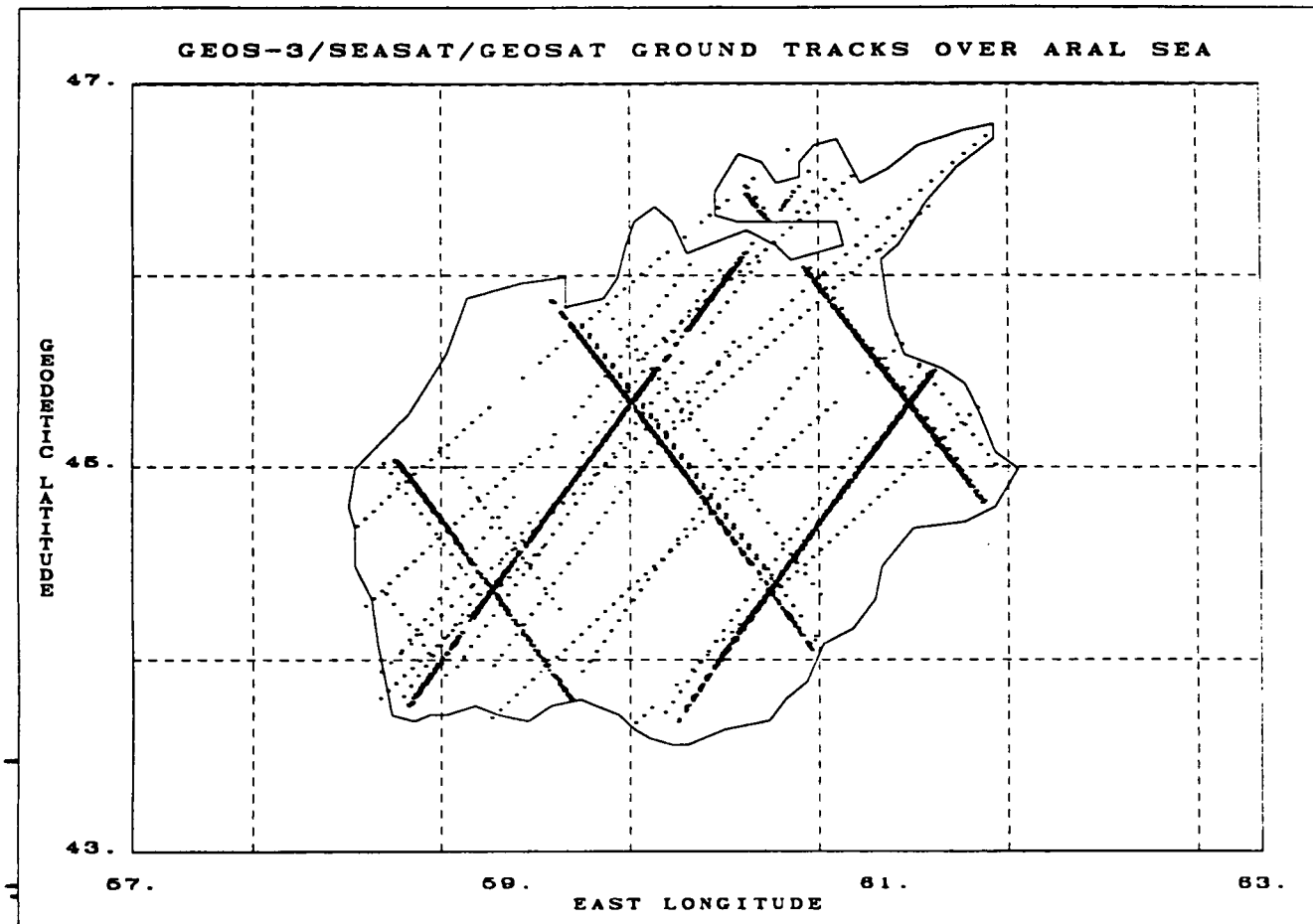


Figure 1. GEOS-3, SEASAT and GEOSAT altimeter data distribution over the Aral Sea.

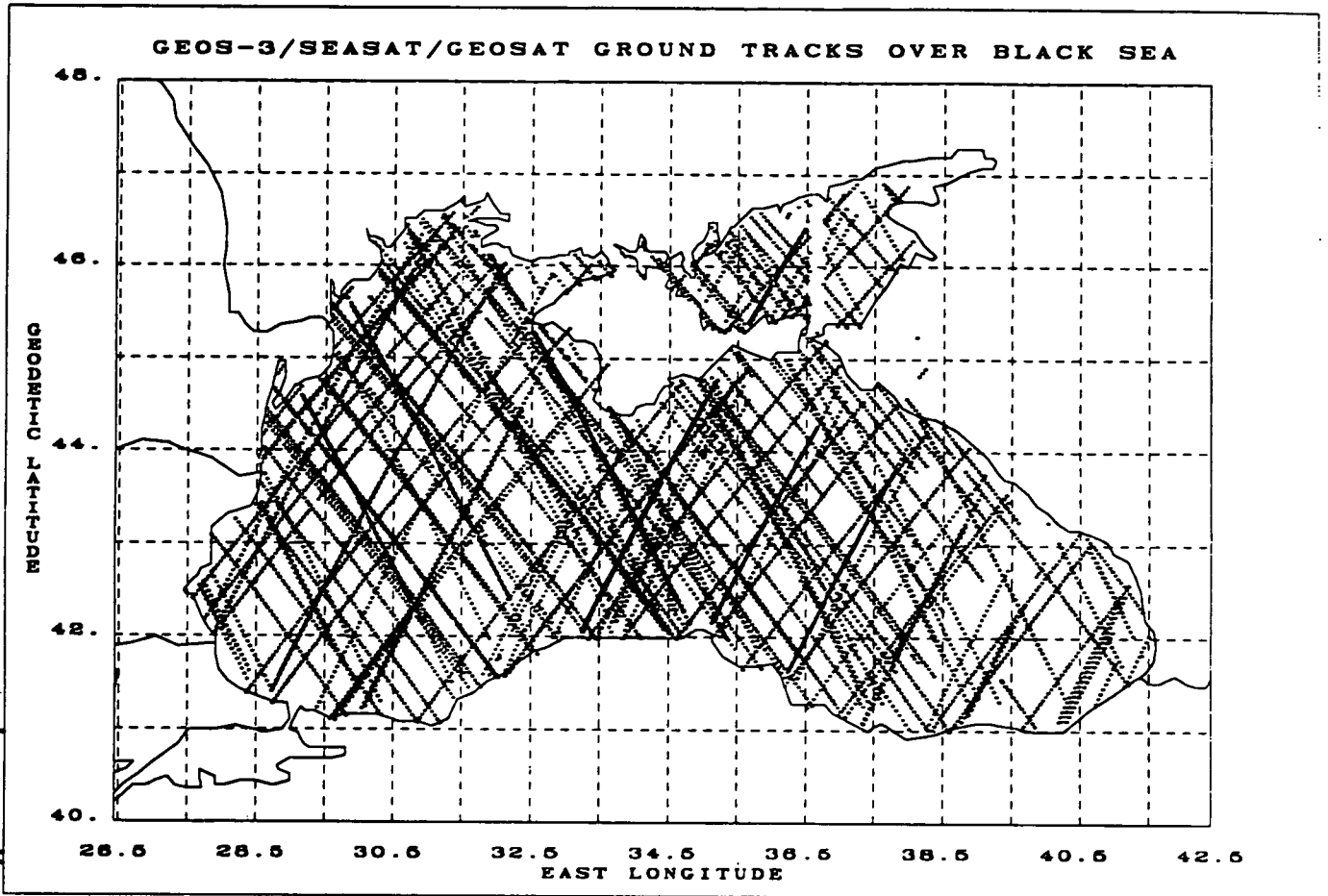
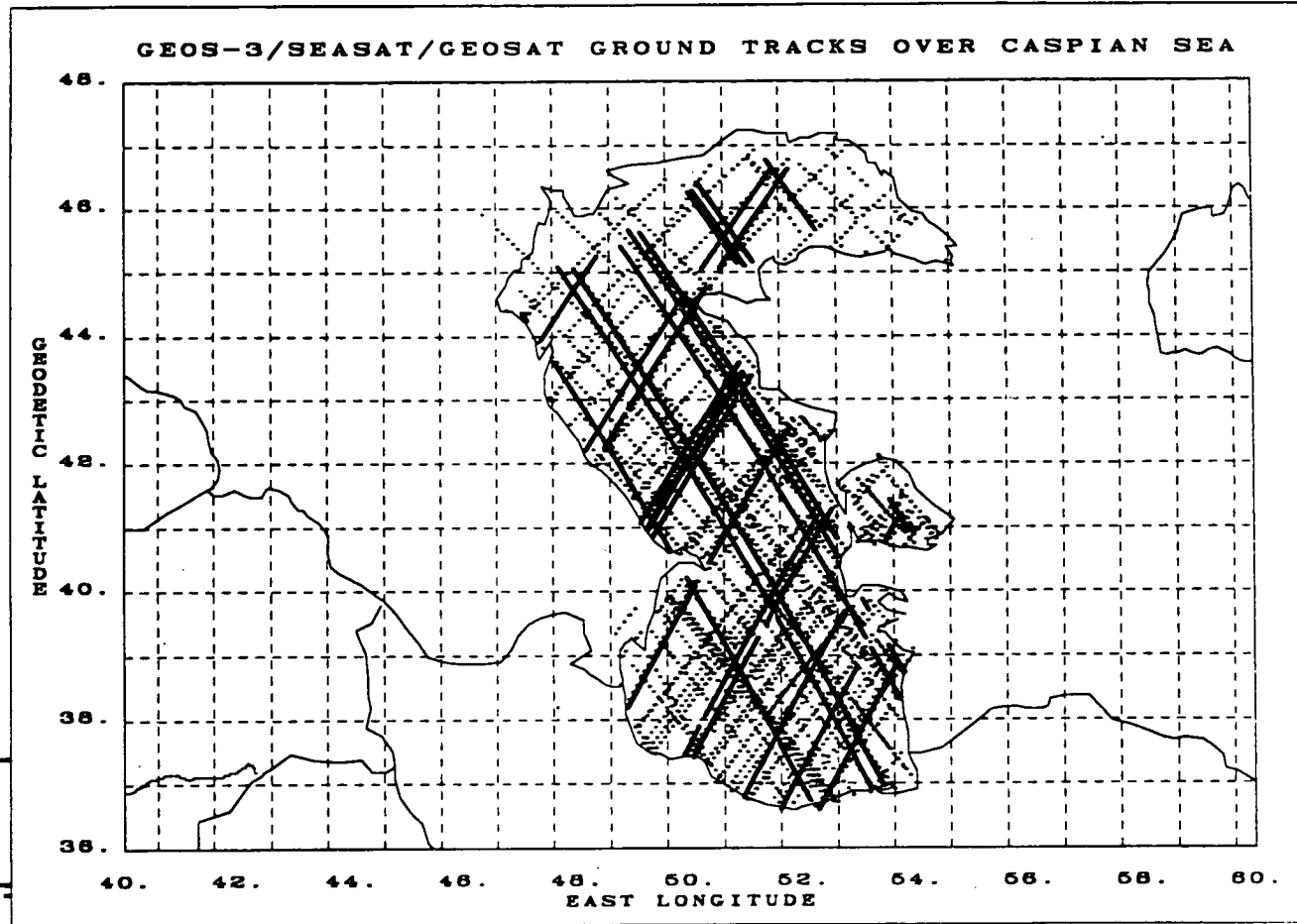


Figure 2. GEOS-3, SEASAT and GEOSAT altimeter data distribution over the Black Sea.



III Figure 3. GEOS-3, SEASAT and GEOSAT altimeter data distribution over the Caspian Sea.

minimized, holding one pass fixed so that all the satellite passes can be defined with respect to a common reference model.

To calculate crossover differences, one must first locate the crossover location in latitude and longitude. There are various methods by which this point can be determined. We have adopted an analytical method of modelling the ground track of the pass. For relatively short arcs, such as the satellite passes over the inland seas, the ground track can be approximated by a second-degree equation,

$$Y = aX^2 + bX + c \quad (1)$$

where  $Y$  and  $X$  are, respectively, the latitude and longitude vectors of ground track records, and  $a$ ,  $b$  and  $c$  are polynomial coefficients to be determined by fitting the ground track data using the method of least-squares. The error in this satellite arc representation is less than 1 Km, which is considerably less than the radius of the illuminated area of the altimeter signal at the sea surface. When the latitudes of the crossover point of two passes,  $Y_1$  and  $Y_2$ , are set equal,  $Y_1 = Y_2$ , the longitude at which this crossover occurs is determined by solving the quadratic equation for  $X$ , subject to the crossover point lying within the latitude and longitude range of the ground-track records of both passes.

Once the crossover point is located, the altimetric height is interpolated by cubic splines from the nearest data for each pass. The true geoid undulation at a crossover point must be the same for both passes regardless of satellite and time. Altimetric height, however, is not exactly the same as geoid undulation. For example, temporal processes such as solid earth and ocean tides may cause the sea-surface height to be different at the different times of the crossing altimeter passes. Ocean tides on small seas like these should contribute less than 10 cm to the crossover difference, but diurnal earth tides may be expected to contribute up to about 30 cm. Fortunately, tides are such broad-scale features in both space and time that they are manifest as a constant bias in a single altimeter pass over small inland seas. Thus any earth tide effects will alias with the orbit error bias and be removed when this bias is adjusted. To illustrate this adjustment, let  $H_l^o$  be the true geoid undulation for pass  $l$  at a crossover point and  $b_l$  be the bias assumed for this pass. The observed geoid undulation  $H_l$  is given by

$$H_l = H_l^o + b_l + \epsilon_l \quad (2)$$

where  $\epsilon_l$  is the random noise at the crossover point for pass  $l$ . The difference  $d_{ij}$  at a crossover point between pass  $i$  and pass  $j$  will be

$$\begin{aligned} d_{ij} &= H_i - H_j \\ &= (H_i^o + b_i + \epsilon_i) - (H_j^o + b_j + \epsilon_j) \\ &= b_i - b_j + (\epsilon_i - \epsilon_j) \end{aligned} \quad (3)$$

because  $H_i^o$  and  $H_j^o$  must be identical at a crossover point. An over-determined system of equations in  $b$  results if all crossovers of each pass with all others are considered. The bias for each pass, therefore, can be determined using the method of weighted least-squares, thus minimizing the crossover differences  $d$ . The standard error is assumed to be 25 cm for GEOS-3, 10 cm for SEASAT and 5 cm for GEOSAT in the weight matrix. The optimal pass bias vector  $B$  is given by

$$B = (\tilde{A}WA)^{-1}(\tilde{A}WD) \quad (4)$$

where  $D$  is the vector of crossover differences,  $W$  is a diagonal matrix in which diagonal elements are the sum of the inverse of the variance of the altimetric data from each satellite. The matrix  $A$  is sparse. Each row of  $A$  contains all zeros except unitary value in the column associated with a pass  $i$  and a negative unitary value in the column associated with pass  $j$ .

The pass with the most crossovers is chosen as the reference pass because it has the most direct influence on other passes. The bias for this pass is not estimated, but, after the crossover-adjustment process, is assigned the average value of the reference surface geoid height along this ground-track, as calculated from a reference geopotential model. Rapp's 180 X 180 model is the reference geopotential model used in the current report. An error covariance matrix of the crossover adjustment was also determined. This error covariance matrix is added to the error associated with each satellite pass to create a more complete error estimate for determining relative data quality in subsequent gridding and gravity prediction operations.

From the geometry of altimeter passes in the current data set, there are at most 2511 crossovers over the Black Sea. These possible crossover locations were carefully checked to eliminate those that coincided with data gaps, which is defined to be part of a satellite arc that did not have an altimeter observation for 70 km, about 10 seconds in time. Such editing reduced the number of crossovers to 2208, 494 of which are GEOS-3 with GEOS-3, 350 are SEASAT with SEASAT, 16 are GEOSAT with GEOSAT, 1000 are GOES-3 with SEASAT, 243 are GOES-3 with GEOSAT and 105 are SEASAT with GEOSAT. The RMS (root-mean-square) of the crossover residuals before bias adjustment is 3.84 m. The RMS after bias adjustment is reduced to 24 cm. The reference pass is the GEOS-3 pass #10557, and its adjusted reference profile and corresponding reference model is shown in Figure 4.

Over the Caspian Sea, there are at most 1380 crossovers. The crossover-selection process described above for the Black Sea was also applied to the Caspian Sea. This reduced the number of crossovers to 1217, 481 of which are GEOS-3 with GEOS-3, 70 are SEASAT with SEASAT, 19 are GEOSAT with GEOSAT, 387 are GOES-3 with SEASAT, 188 are GOES-3 with GEOSAT and 72 are SEASAT with GEOSAT. The RMS of the crossover residuals before bias adjustment is 2.19 m, and reduced to 28 cm after bias adjustment. The reference pass is the SEASAT pass #832, and its adjusted reference profile and corresponding reference model is shown in Figure 5.

Over the Aral Sea, there are at most 3220 crossovers. The crossover-selection process

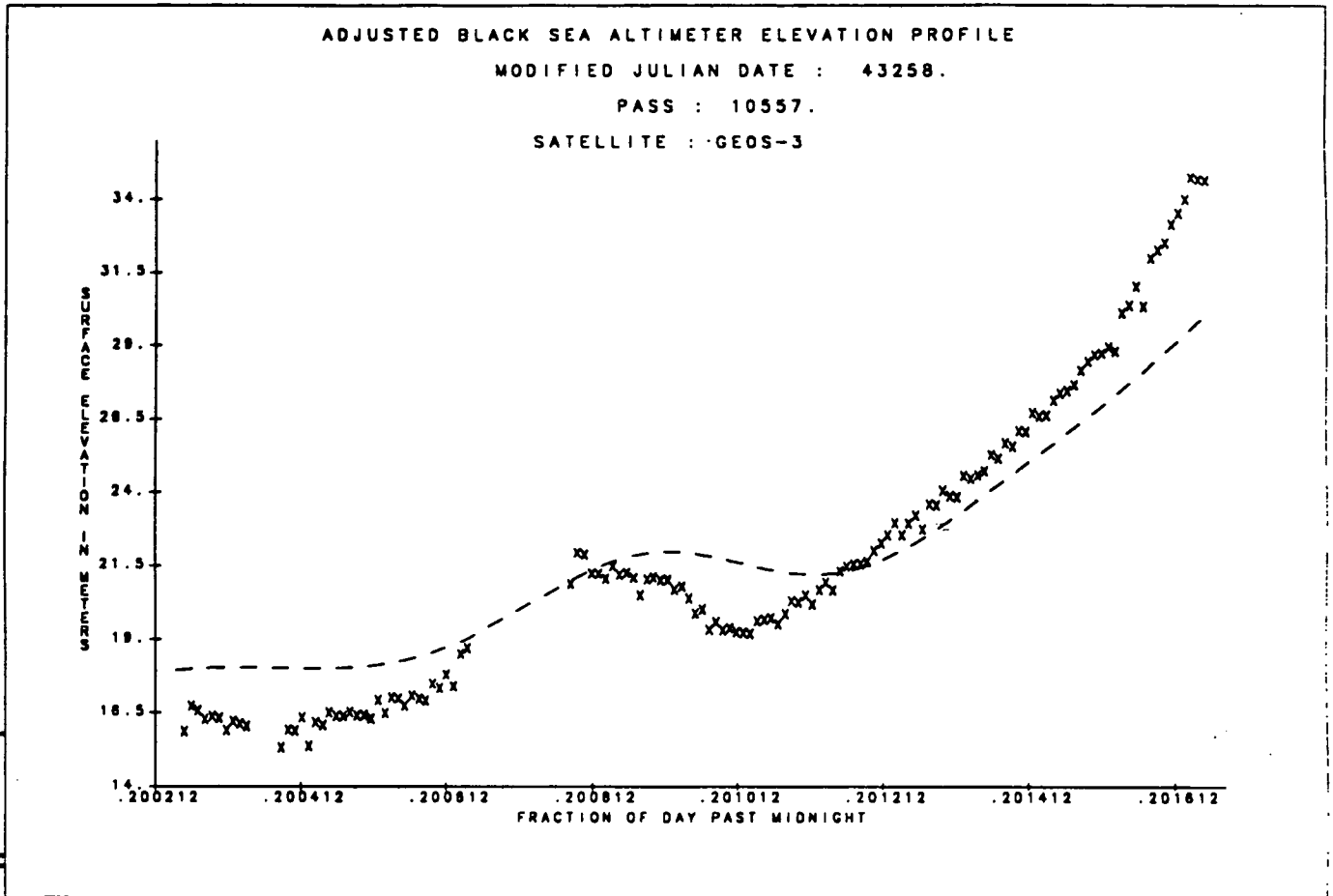


Figure 4. Sample adjusted altimeter elevation profiles of the Black Sea. Profile of the reference pass. Dashed line is Rapp's 180 X 180 reference geoid.



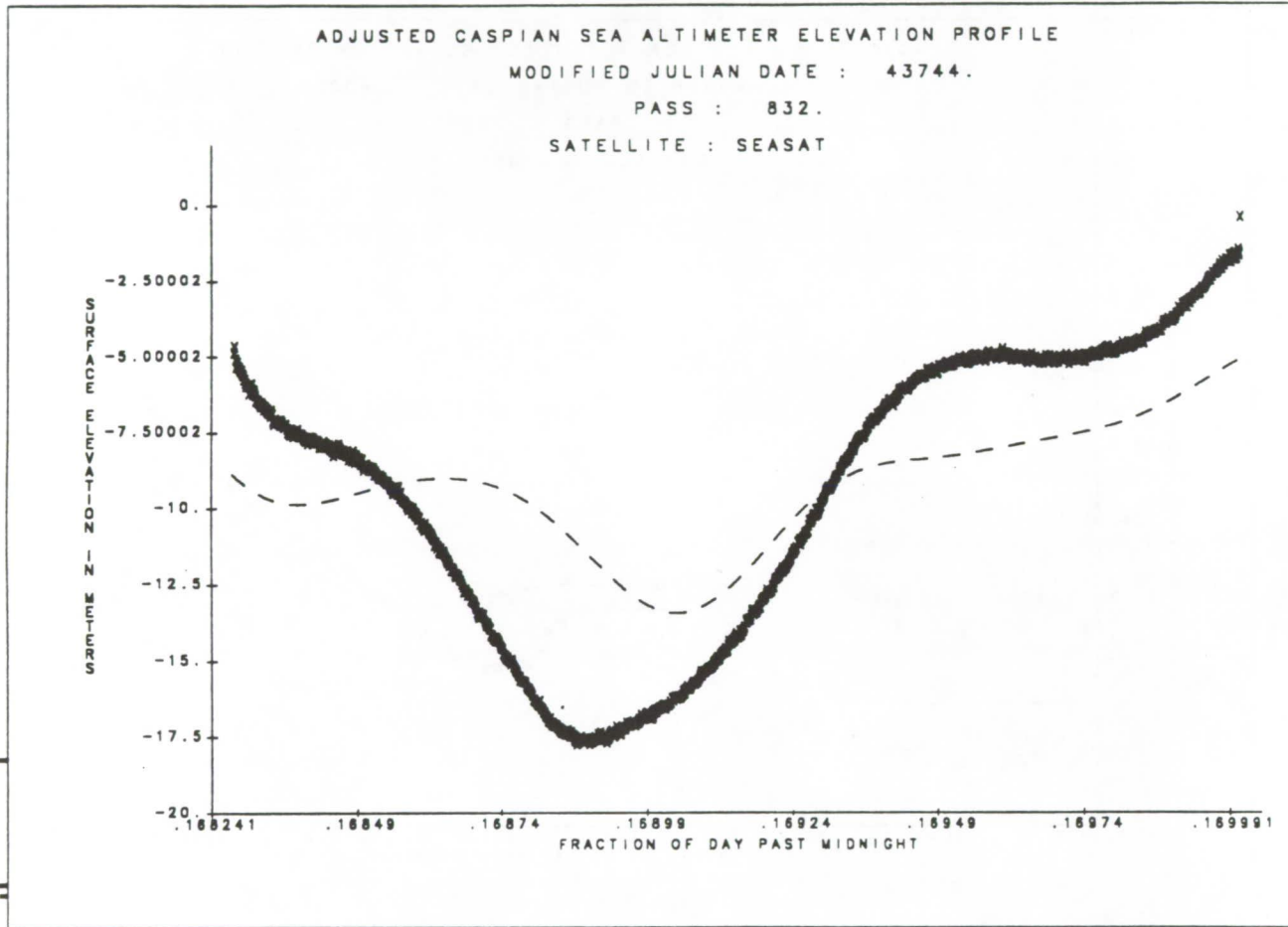


Figure 5. Sample adjusted altimeter elevation profiles of the Caspian Sea. Profile of the reference pass. Dashed line is Rapp's 180 X 180 reference geoid.

was applied to the Aral Sea data set, and ten passes that cross no other passes were also removed. This reduced the total number of crossovers to 1136, none of which is GEOS-3 with GEOS-3, 30 are SEASAT with SEASAT, 803 are GEOSAT with GEOSAT, 17 are GOES-3 with SEASAT, 85 are GOES-3 with GEOSAT and 201 are SEASAT with GEOSAT. The RMS of the crossover residuals before bias adjustment is 5.70 m, whereas the RMS after bias adjustment is reduced to 17 cm. This reduced level of crossover error is to be expected given the preponderance of high-quality GEOSAT-GEOSAT crossovers. The reference pass is the GOES-3 pass #6547. The adjusted reference profile and its corresponding reference model is shown in Figure 6.

After the data were corrected for pass biases, an overall bias representing the average difference in height between the reference pass and the reference geoid is added to the data. For the Aral Sea data, the adjustment was about 50 m, for the Black Sea, 2 m and for the Caspian Sea, -34 m. Some of this adjustment undoubtedly represents the height of the inland sea above or below mean-sea level (the geoid) as well as an arbitrary level of orbit error in the reference pass.

### III. APPLICATION OF COLLOCATION TECHNIQUE

Collocation is a predictive method based on linear least-squares interpolation, in which a stochastic spatially averaged correlation between observables in the data space is assumed. An auto-correlation function, which reflects a spatial correlation of observables in a data space, is used for the purpose of interpolation. For transformations from a data space into a prediction space, a cross-correlation function, which represents the spatial correlation between variables in the data space and the prediction space, is required. In least-squares collocation procedure, these correlation functions are the geoid-geoid, geoid-gravity and gravity-gravity covariance functions. A general description of collocation can be found in Moritz (1978). A brief review of the collocation method relevant to the subsequent analysis is given in Au *et al.* (1989a).

#### Collocation Gridding of Geoid Undulations

According to the linear least-squares interpolation formula, the predicted geoid undulation  $N(P)$  at a point  $P$  is given by

$$N(P) = C_{PN}(C_{NN}+D)^{-1}N_p \quad (5)$$

where  $C_{PN}$  is a covariance vector relating the undulation at  $P$  to the observable in the neighborhood of  $P$ ,  $C_{NN}$  is the stochastic undulation covariance matrix,  $D$  is the error covariance matrix that represents the random error associated with each observable and the error from crossover adjustments, and  $N_p$  is a column vector of geoid undulation observables in the neighborhood of  $P$ . The stochastic undulation covariance matrix is derived from a geoid-geoid auto-correlation function that reflects the averaged roughness and topographic correlation of the region concerned. The averaged roughness is manifest in the form of a covariance amplitude, whereas the topographic correlation is represented

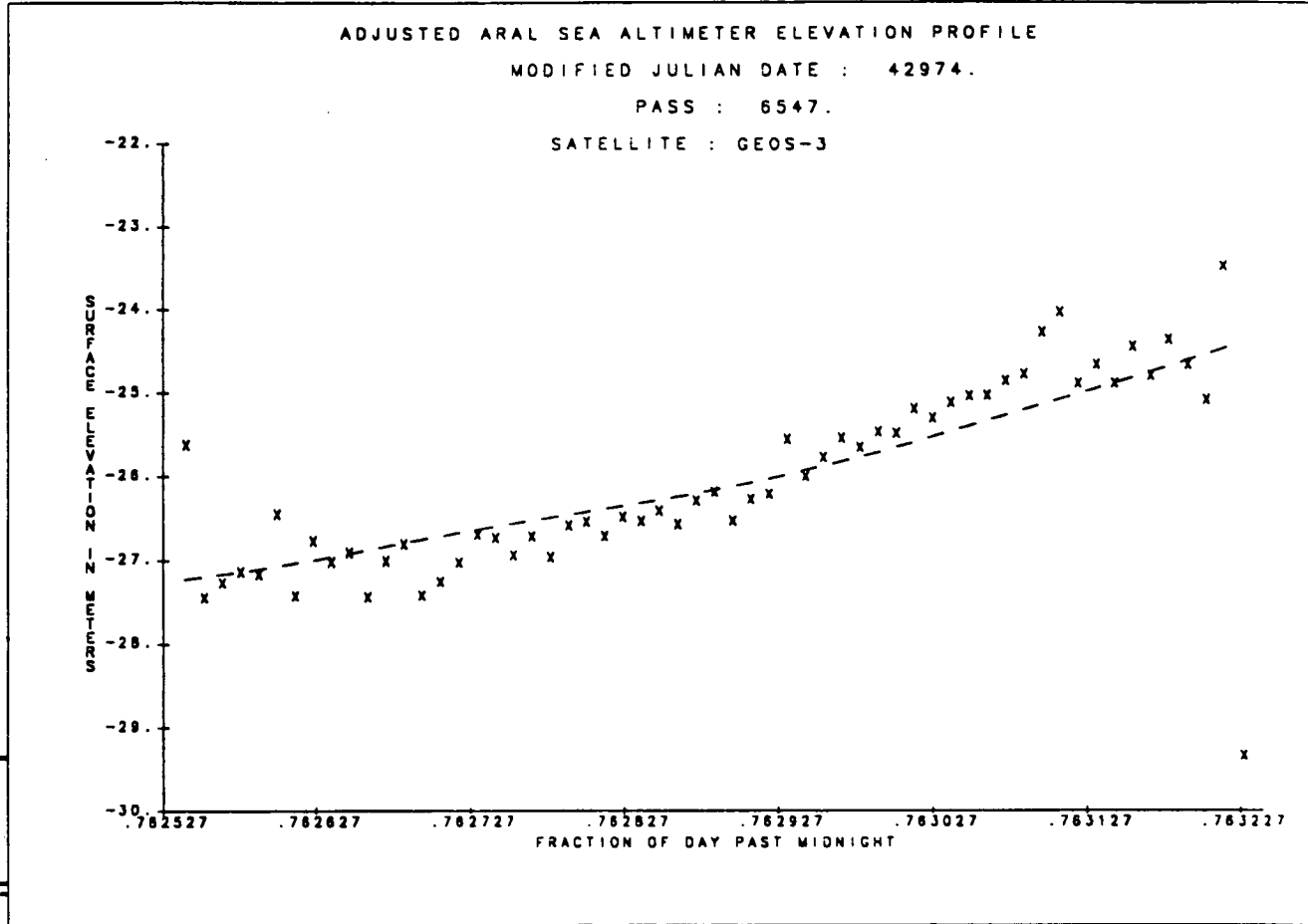


Figure 6. Sample adjusted altimeter elevation profiles of the Aral Sea. Profile of the reference pass. Dashed line is Rapp's 180 X 180 reference geoid.

by a correlation length. In essence, the collocation method assigns a weight to each observable via the stochastic covariance matrix in a weighted-average process. For example, if the weights are assigned as a function of the inverse of the square of distance from the point at which prediction is made, the collocation results coincide with those derived from weighted-averages based on the inverse of the square of distance. The variance at the interpolated point is given by

$$\sigma^2 = C_o - C_{PN}(C_{NN})^{-1}C_{PN} \quad (6)$$

where  $C_o$  is the square of the geoid-geoid covariance amplitude.

A variety of covariance functions have been used in the collocation process. Commonly-used covariance functions are the global covariance functions due to Rapp's 180 X 180 global reference geopotential model (Rapp, 1986), the theoretical self-consistent covariance functions due to Jordan (Jordan, 1972) and local empirical covariance functions derived for a specified region (Knudsen, 1987, 1988; Au *et al.*, 1989a, 1990). The effects of a particular choice of covariance functions on both geoid interpolation and geoid-to-gravity transformation for local areas such as the Aral Sea, the Black Sea and the Caspian Sea are discussed in Au *et al.* (1990, 1989a). Comparing the geoid results based on Rapp's global covariance function with those based on the local empirical and the hybrid Jordan's covariance functions (Au *et al.*, 1989a, 1990), it is noted that geoid interpolation is rather insensitive to the choice of covariance functions even when the covariance functions are very different. For example, the correlation length of the Rapp's covariance functions is about 1.3°, whereas that of the local empirical covariance functions is about 0.1° for the Black Sea. The corresponding covariance amplitudes are 1 m for Rapp's geoid-geoid covariance function and 1.6 m for the local empirical geoid-geoid covariance function. However, in the altimetry analysis over the Aral, the Black and the Caspian Seas, Au *et al.* (1990, 1989a) found that the results of gravity prediction from geoid data are sensitive to the choice of covariance functions.

A local empirical residual covariance function can be determined based on the difference between gridded weighted-average geoid undulations (Au *et al.* 1989a, 1990) and the reference geoid derived from Rapp's 180 X 180 reference geopotential model. An empirical computation technique described by Moritz (1978) is used to determine this local residual covariance function, which is constructed by the convolution of the difference between the weighted-average geoid data and the reference geoid. The resultant covariance function is, in effect, a least-squares filter (Treitel and Robinson, 1966), which determines the contribution of each observable to the predicted value at a grid point. Plots of local empirical geoid-geoid covariance functions for the Aral Sea, the Black Sea and the Caspian Sea are shown, respectively, in Figures 7, 8 and 9. Contour maps of the geoid undulations of the Aral Sea, the Black Sea and the Caspian Sea, gridded with local empirical covariance functions are shown, respectively, in Figures 10, 11 and 12.

The contour maps of the geoid undulations according to the reference geopotential model, Rapp's 180 X 180 model, of the Aral Sea, the Black Sea and the Caspian Sea are shown in Figures 13, 14 and 15, respectively. For the Black Sea, the gridded geoid

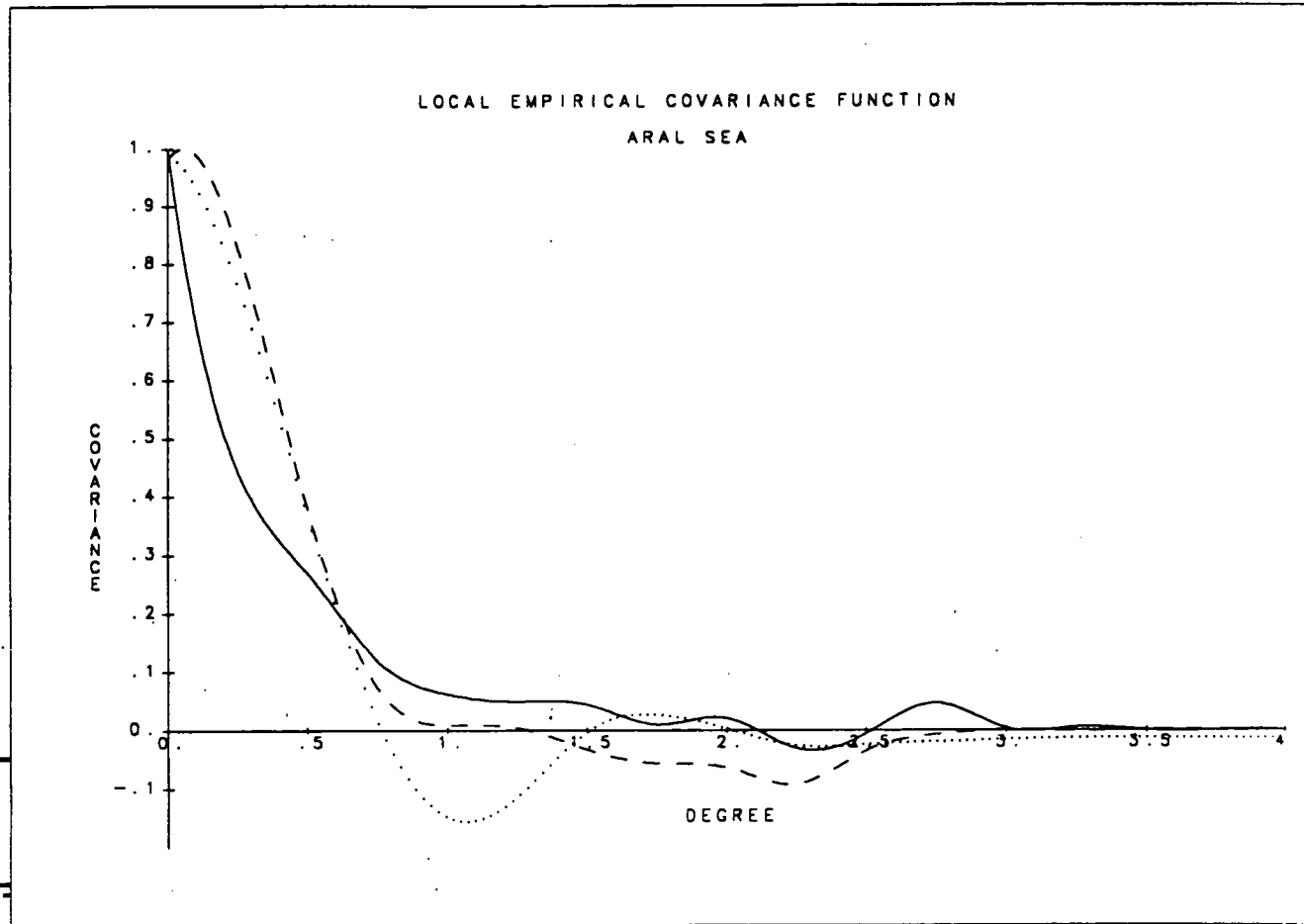


Figure 7. Normalized local residual empirical covariance functions of the Aral Sea. The normalization coefficients for:

- 1) geoid-geoid (solid line) is  $3.27 \text{ m}^2$ ,
- 2) geoid-gravity (dashed line) is  $23.48 \text{ m-mgal}$ , and
- 3) gravity-gravity (dotted line) is  $826.17 \text{ (mgal)}^2$ .

LOCAL EMPIRICAL COVARIANCE FUNCTION  
BLACK SEA

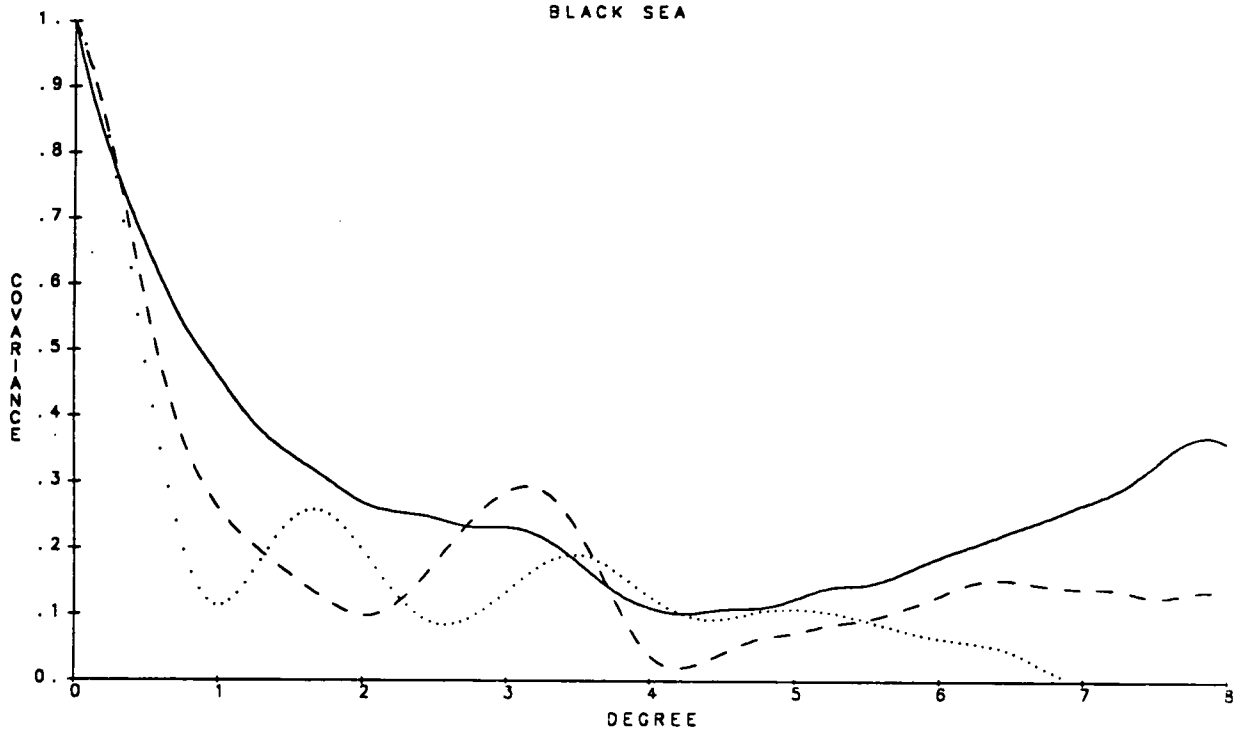


Figure 8. Normalized local residual empirical covariance functions of the Black Sea. The normalization coefficients for:

- 1) geoid-geoid (solid line) is  $1.61 \text{ m}^2$ ,
- 2) geoid-gravity (dashed line) is  $9.76 \text{ m-mgal}$ , and
- 3) gravity-gravity (dotted line) is  $173.2 \text{ (mgal)}^2$ .

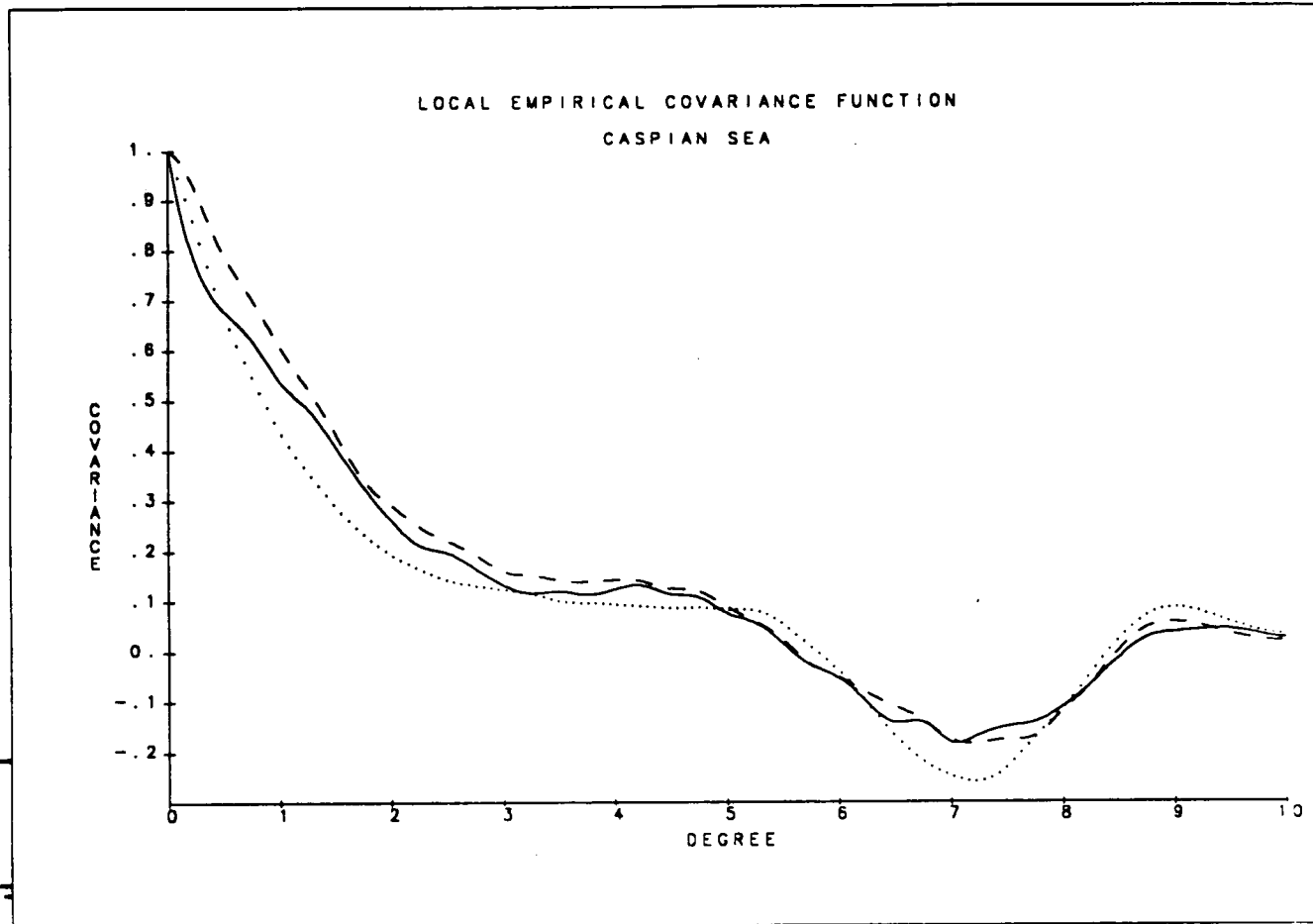


Figure 9. Normalized local residual empirical covariance functions of the Caspian Sea. The normalization coefficients for:

- 1) geoid-geoid (solid line) is  $8.86 \text{ m}^2$ ,
- 2) geoid-gravity (dashed line) is  $44.11 \text{ m-mgal}$ , and
- 3) gravity-gravity (dotted line) is  $345.8 \text{ (mgal)}^2$ .

III

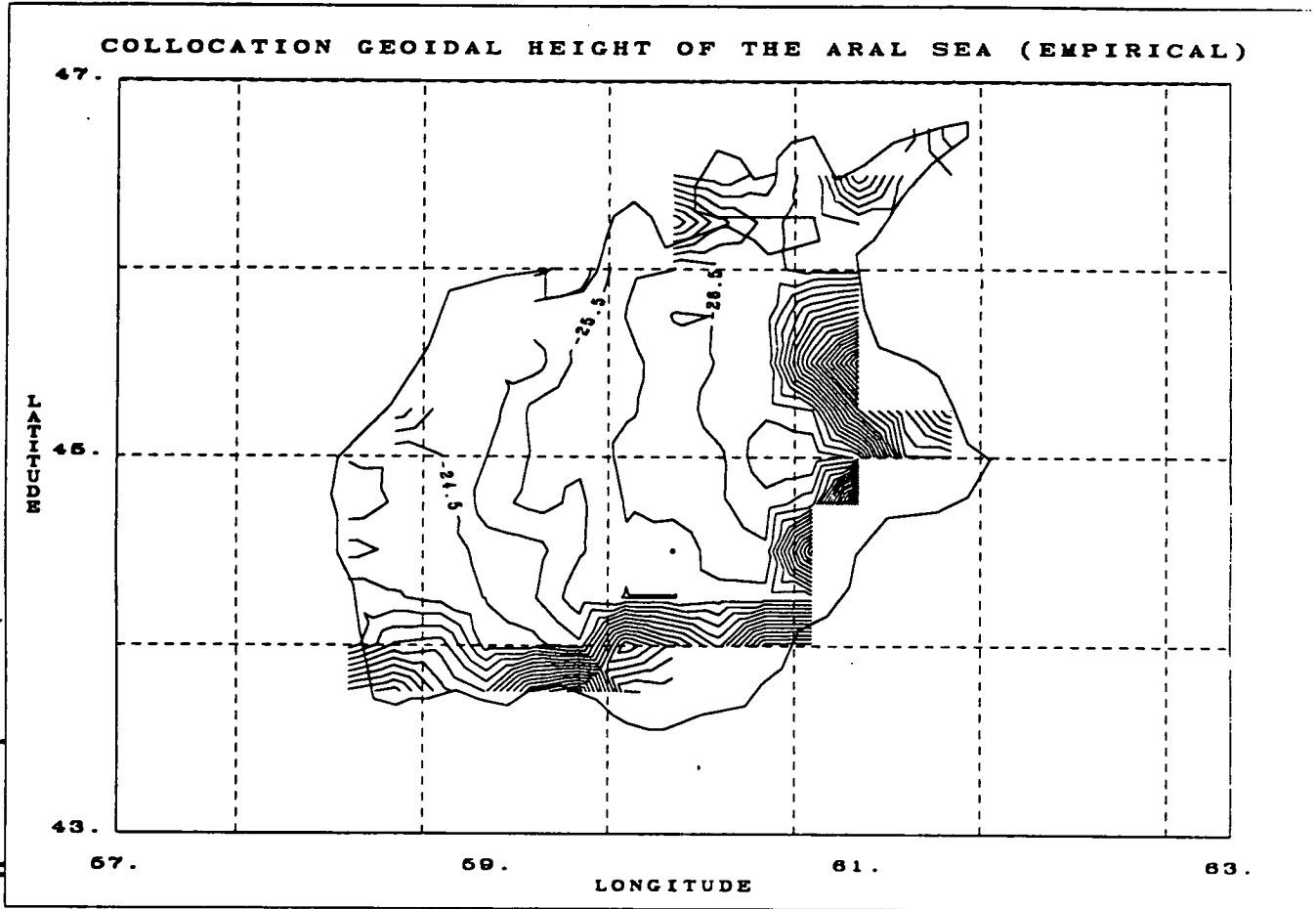
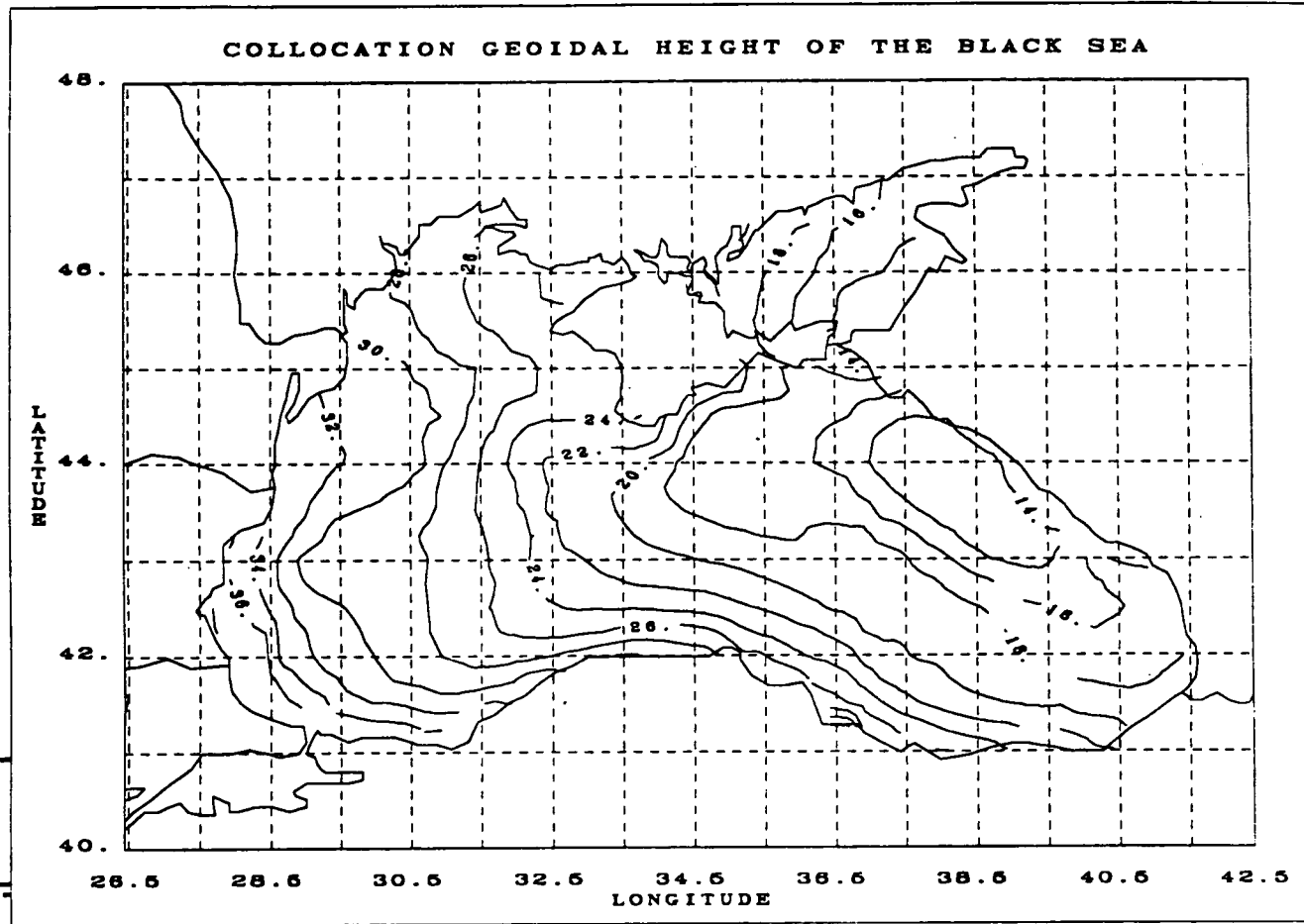


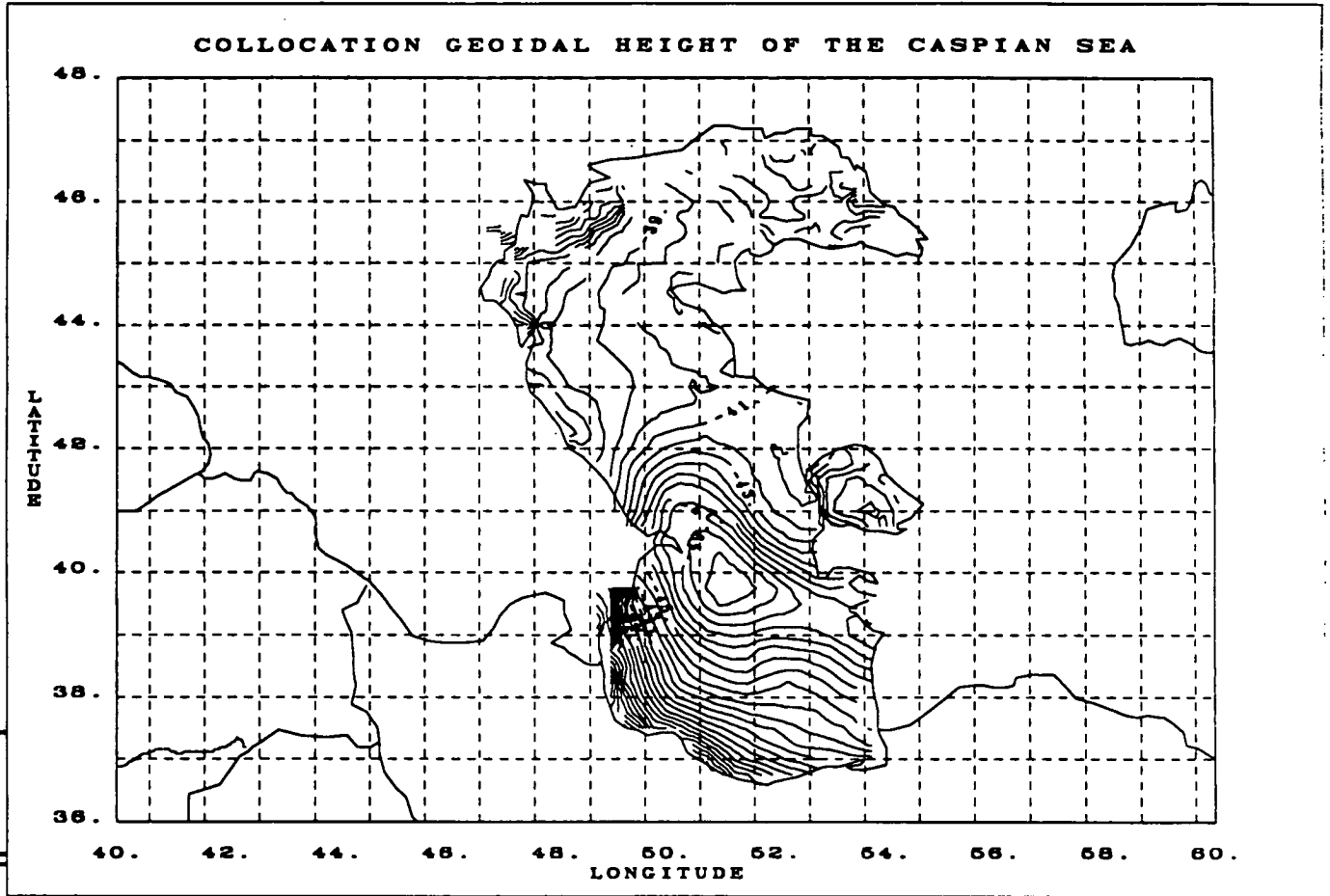
Figure 10. A contour map of the collocation geoid undulations of the Aral Sea (m above mean sea level) gridded with local empirical geoid-geoid covariance function.



11



11 Figure 11. A contour map of the collocation geoid undulations of the Black Sea (m above mean sea level) gridded with local empirical geoid-geoid covariance function.



ii Figure 12. A contour map of the collocation geoid undulations of the Caspian Sea (m above mean sea level) gridded with local empirical geoid-geoid covariance function.

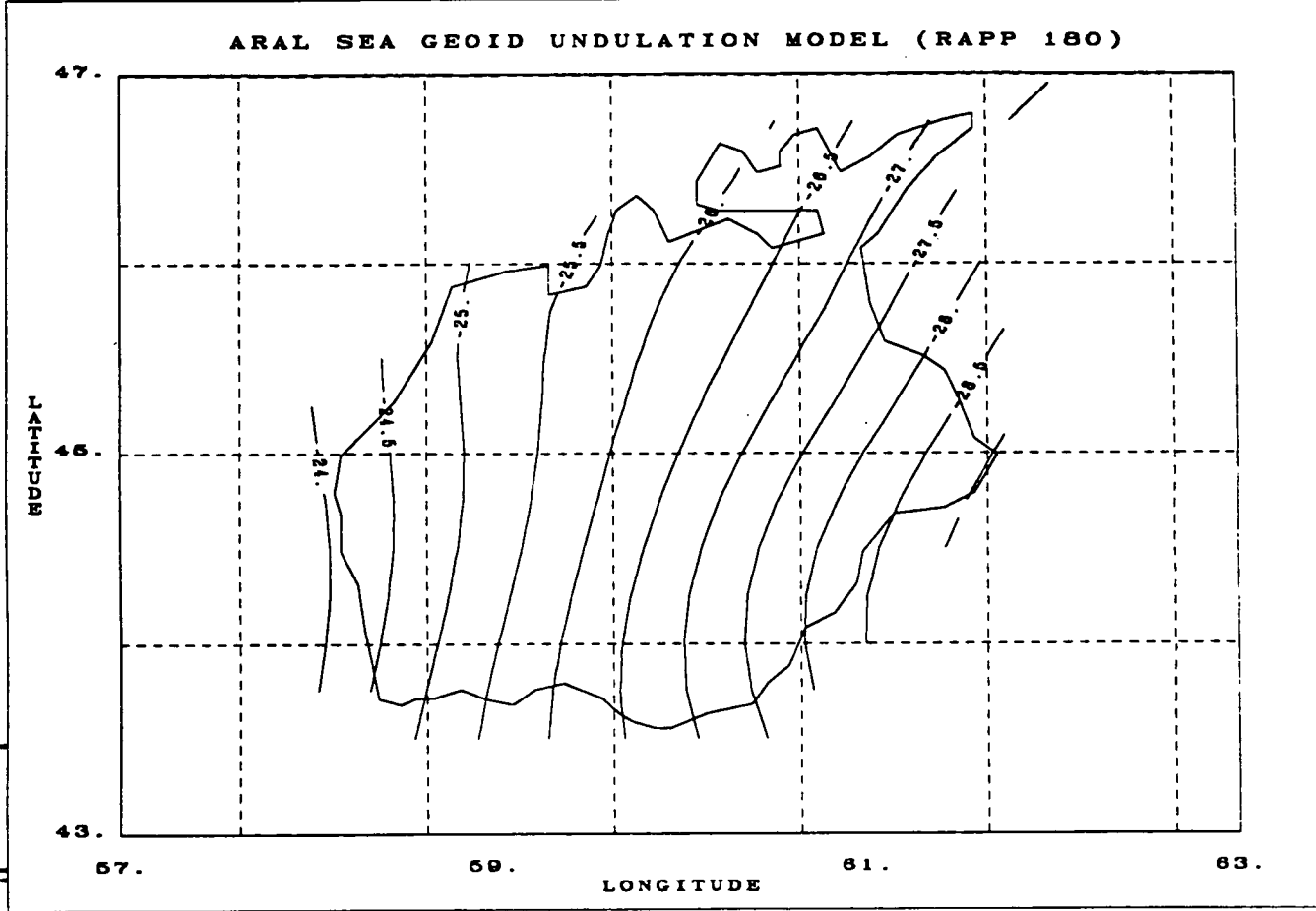


Figure 13. A contour map of Rapp's 180 X 180 reference geoid undulations (m above mean sea level) of the Aral Sea.

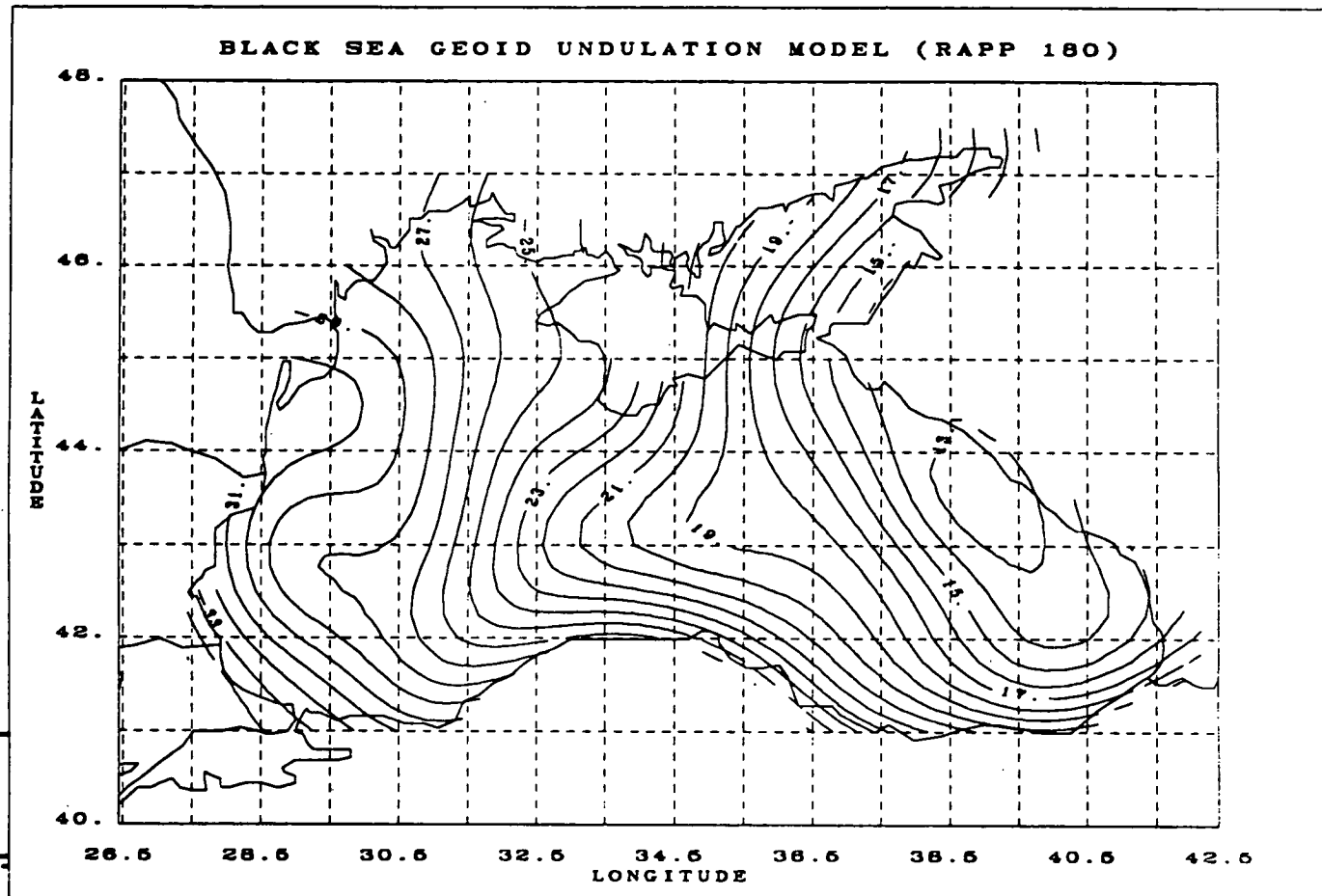
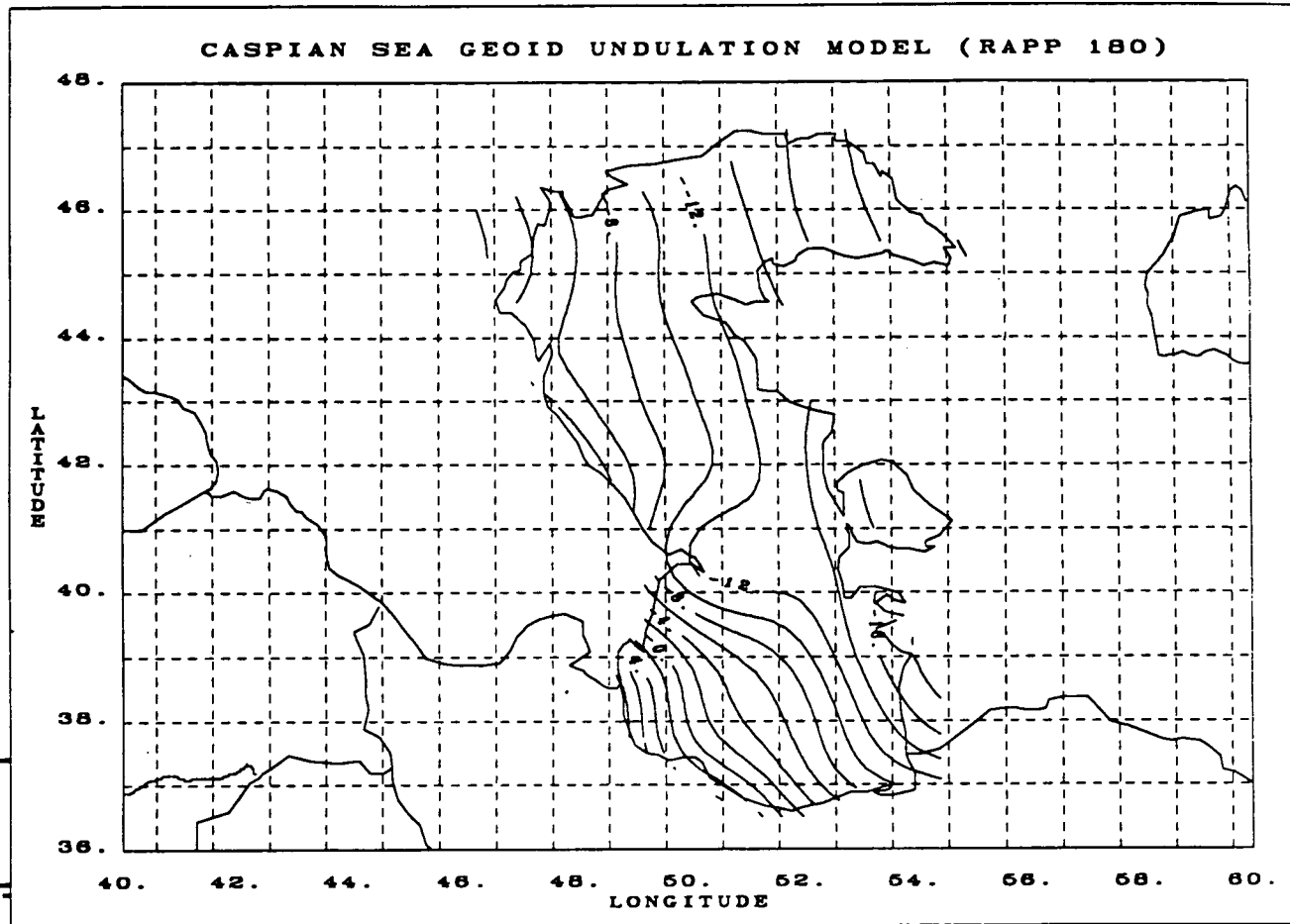


Figure 14. A contour map of Rapp's 180 X 180 reference geoid undulations (m above mean sea level) of the Black Sea.

11



11 Figure 15. A contour map of Rapp's 180 X 180 reference geoid undulations (m above mean sea level) of the Caspian Sea.

closely resembles the corresponding reference geoid. On the other hand, the gridded geoids of both the Aral and the Caspian Seas deviate substantially from the corresponding reference geoids. For example, considerable structure and steep gradients are observed at the eastern and southern parts of the Aral Sea and at the southern part of the Caspian Sea. Obviously, there is more short-wavelength information in the reference geoid undulation model of the Black Sea than in the models of the Aral and the Caspian Seas. The information content of a reference geopotential model has considerable effect on the quality of gravity anomalies results transformed from geoid undulation data, as will be seen later.

The estimated errors (square root of the variance) associated with the interpolated geoid of the Aral Sea, the Black Sea and the Caspian Sea, are 40 cm, 20 cm and 40 cm. Note from Figures 1-3 that the estimated errors in the gridded data vary inversely with the density of ground tracks and is much smaller for the Black Sea than for both the Aral Sea and the Caspian Seas. This disparity in error values reflects somewhat the difference in the covariance amplitudes of the local empirical covariance functions used and the larger crossover error over both the Aral and the Caspian Seas, but mostly the less uniform and sparser data distribution over the Aral and the Caspian Seas.

### **Estimation of Gravity Anomalies**

Analogous to the collocation interpolation above, geoid undulations can be transformed into gravity anomalies (Rapp, 1986) according to the equation

$$\Delta g = C_{gN}(C_{NN}+D)^{-1}(N-N_R) + \Delta g_R \quad (7)$$

where  $\Delta g$  is the predicted point gravity anomaly,  $C_{gN}$  is the covariance vector of geoid-to-gravity transformation,  $C_{NN}$  is the covariance matrix for geoid-geoid interpolation,  $D$  is the error covariance matrix that is constructed from the variance of the interpolation of geoid undulations,  $N$  is the vector of gridded geoid undulations,  $N_R$  is the vector of reference model geoid undulations that corresponds to each observed value of  $N$ , and  $\Delta g_R$  is the reference model gravity anomaly value at the predicted grid point. The first term in equation (7) can be regarded as a perturbation on the reference gravity anomalies by the deviation of the observed geoid from the reference geoid. The variance of the gravity prediction is given by

$$\sigma^2 = C_{gg} - C_{gN}(C_{NN}+D)^{-1}C_{gN} \quad (8)$$

where  $C_{gg}$  is the square of the gravity-gravity covariance amplitude. The input data for the geoid-to-gravity transformation are the collocation-gridded geoid undulations and their corresponding variances. Use of a gridded data set greatly reduced the strain on computer resources because it contains far fewer data points than the original altimeter tracks.

A literature search on collocation techniques and local covariance functions for the geoid and gravity anomalies reveals that local covariance functions vary markedly from one area to another. Thus, it should not be a surprise that a single covariance function does

not perform equally well for all three inland seas. In order to perform the geoid-to-gravity transformation accurately in each sea, a locally valid geoid-to-gravity covariance function must first be obtained. But the information we need to construct a locally valid covariance function is exactly that which is to be predicted by the collocation exercise in equation (7). To resolve this classic "chicken and egg" dilemma, approximate local gravity anomalies for an inland sea are first predicted using Rapp's global covariance functions (shown in Figure 16) and the gridded geoid data. Based on this approximate local empirical gravity-anomaly information, a set of local empirical covariance functions (shown in Figures 7, 8 and 9) for the Aral Sea, the Black Sea and the Caspian Sea are derived by numerical convolution.

A set of covariance functions (geoid-geoid, geoid-gravity and gravity-gravity) describes the physical relationships such as surface roughness and topographical phase relations between the gravity field and the geoid undulations. In general, there is more high-frequency information in the gravity field than in the geoid undulations, because gravity is a derivative of the geoid. Thus, the correlation distance (the half-height length of the gravity-gravity covariance functions) is shorter than that for the geoid-geoid and geoid-gravity covariance functions, as is shown in the set of covariance functions for the Black Sea. This systematic relationship is implicitly observed in Rapp's global covariance functions, and explicitly expressed in Jordan's theoretical self-consistent covariance functions. Ideally, locally derived empirical covariance functions should also reflect this systematic relationship. However, this will not be the case if local high-frequency information is unavailable due to lack of surface observations. This scenario is exemplified in the set of local empirical covariance functions for the Caspian Sea (see Figure 9), which are practically identical except for their covariance amplitudes. The reason for these anomalous properties is not known exactly, but it is suspected that the quality of the reference model in the vicinity of the Caspian Sea is of critical importance. We note that the empirical covariance functions for the Black Sea behave normally, and there is close agreement between the observed geoid and the model geoid over the Black Sea, in contrast to the striking differences between the observed and model geoids over the Caspian Sea. Over the Black Sea, accurate short-wavelength geopotential information has been incorporated in Rapp's 180 X 180 geopotential reference model. The altimeter measurements, represented by the gridded geoid heights, add little new information. This is not the case, however, for the Caspian Sea. It is suspected that the accurate high-frequency information that was included in Rapp's 180 X 180 geopotential model for the Black Sea is absent for the Caspian Sea. For such a local region, where high-frequency surface observations are not available, hybrid local empirical covariance functions based on Jordan's formulation and using locally derived covariance parameters (covariance amplitudes and correlation length) is a logical choice. A set of hybrid covariance functions for the Caspian Sea are shown in Figure 17. A benchmark test of the viability of such a hybrid collocation technique has been performed (Au *et al.*, 1989a). The quality of the transformation from geoid undulations to gravity anomalies varies depending on the frequency content of the reference geopotential model, calling into question the robustness of the transformation.

The peak amplitude of the Aral Sea local empirical geoid-gravity covariance function (see Figure 7), however, is offset from the origin by about  $0.1^\circ$  (a case of the split maxima). It

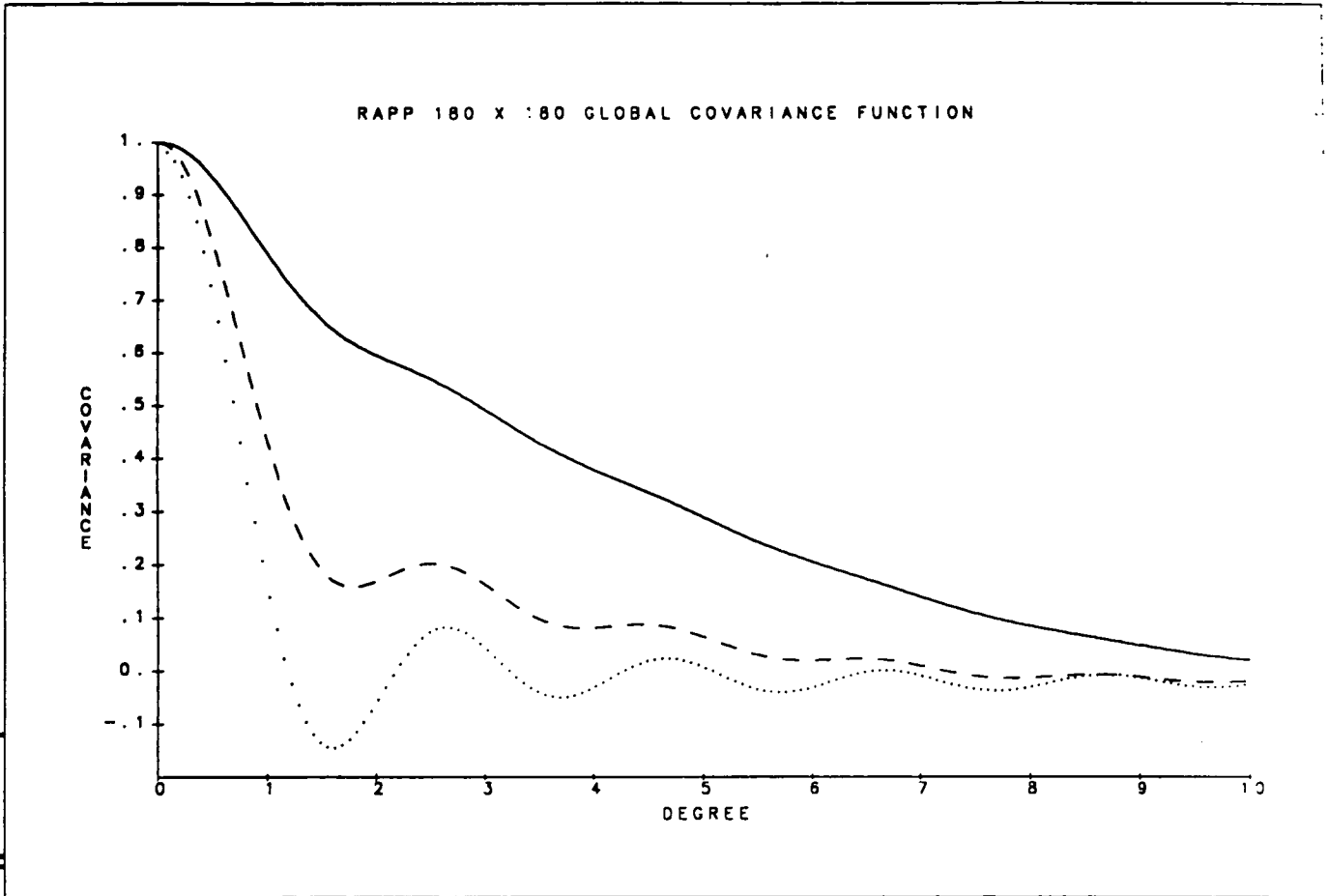
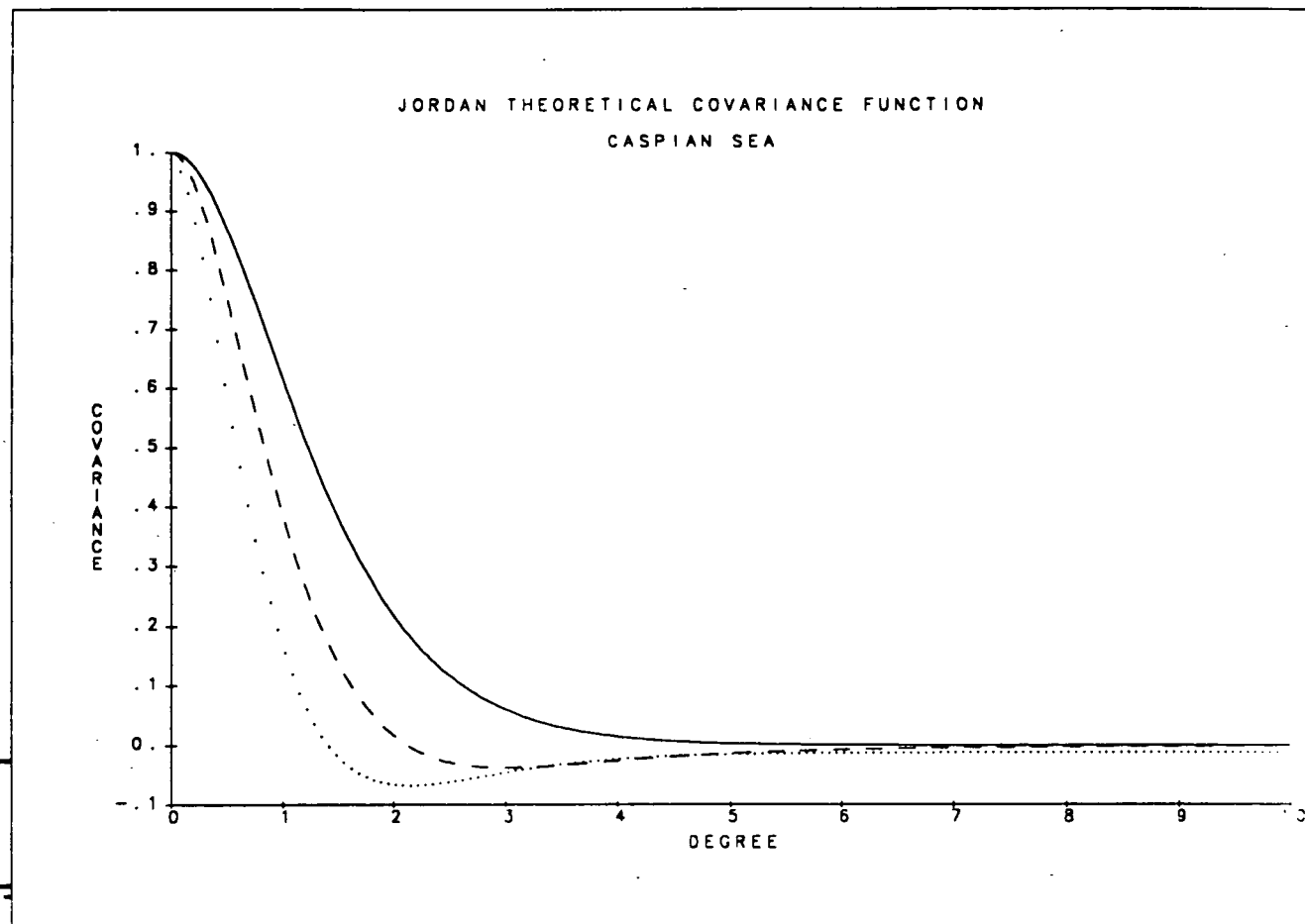


Figure 16. Normalized Rapp's 180 X 180 global covariance functions. The normalization coefficients for:

- 1) geoid-geoid (solid line) is  $1.13 \text{ m}^2$ ,
- 2) geoid-gravity (dashed line) is  $7.26 \text{ m-mgal}$ , and
- 3) gravity-gravity (dotted line) is  $98.36 \text{ (mgal)}^2$ .





1 Figure 17. Normalized Jordan's theoretical covariance functions of the Caspian Sea. The normalization coefficients for:

- 1) geoid-geoid (solid line) is  $8.86 \text{ m}^2$ ,
- 2) geoid-gravity (dashed line) is  $45.20 \text{ m-mgal}$ , and
- 3) gravity-gravity (dotted line) is  $345.8 (\text{mgal})^2$ .

may be that this anomaly is an artifact caused by the limited extend of the region involved in the convolution process. In other disciplines, split maxima in correlation functions reveal underlying special symmetries in the pre-convoluted functions. For example, planar twinning in crystals can be deduced from the split maxima in its crystallographic correlation function (Cowley and Au, 1978). The split maximum in our geodetic covariance function may be related to the symmetries of the reference geoid surface and reference gravity-anomaly surface. The reference geoid surface (see Figure 13) approximates an inclined plane, whereas the reference gravity-anomaly surface (see Figure 21) is basically a saddle with the ridge running northeast to southwest. This special geometry may be manifest as a split maximum in the cross-correlation function. Such special geometry of the Aral Sea is not seen in the conventional Rapp's global covariance functions nor in Jordan's self-consistent covariance functions because the Rapp's and Jordan's covariance functions are derived according to models, not according to local topographic symmetries. This sensitivity to local geometry, if true, further justifies use of the local empirical covariance functions for both geoid gridding and gravity prediction for the Aral Sea.

Contour maps of the predicted gravity anomalies of the Aral Sea and the Black Sea using local empirical covariance functions and a contour map of the predicted gravity anomalies of the Caspian Sea using hybrid local empirical covariance functions are shown, respectively, in Figures 18, 19 and 20. The corresponding estimated errors in the gravity prediction are about 24 mgal, 10 mgal and 8 mgal respectively for the Aral, Black, and Caspian Seas. Again, the disparity in error values mirrors the difference in the covariance amplitudes of the local empirical covariance functions used and the larger variances of the geoid interpolation for the Aral Sea due to the less uniform and sparser data distribution over the Aral Sea. Contour maps of the Aral Sea, Black Sea and Caspian Sea reference gravity anomalies based on Rapp's 180 X 180 model are shown, for comparison, in Figures 21, 22 and 23, respectively. Comparing Figures 18-20 with Figures 21-23, we see that the geoid-to-gravity transformation adds high-frequency gravity information over and above that in the reference models. The geophysical significance of the results will be discussed in a later section.

#### **IV. ROBUSTNESS TEST FOR THE GEOID-TO-GRAVITY TRANSFORMATION**

A review of the literature for covariance functions indicated that the correlation distance of Rapp's geoid undulation covariance function is much too long, at 3 arc degrees, to be valid for areas as small as the inland seas. Models by Knudsen (1987) and by Jordan (1972) indicated a correlation distance for the geoid beyond degree 180 of 0.33 and 0.45 arc degrees, respectively. Correlation distance parameters for the gravity covariance function and the cross-covariance function also appeared too long, but not by so great a factor. As a trial, Jordan's self-consistent set of covariance function formulas were used, setting the geoid function correlation length to 0.5 arc-degrees, with the result that the estimated gravity anomalies have a closer resemblance to the reference gravity model, and the inverse transformation yielded the original geoid (Au *et al.*, 1989a). A consistency test was designed, then, to study the sensitivity of the geoid-to-gravity

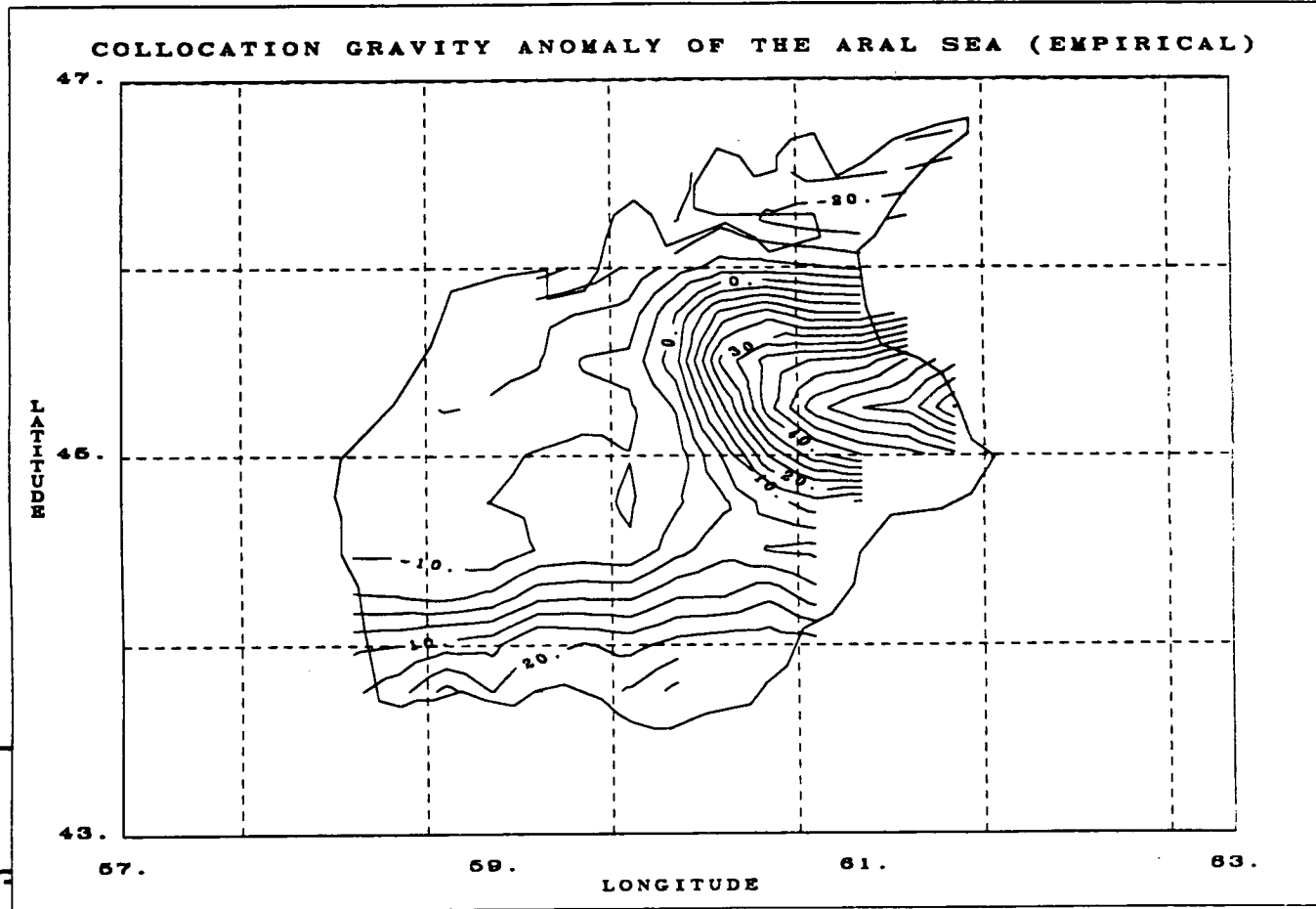


Figure 18. A contour map of estimated gravity anomalies (mgal) of the Aral Sea predicted with local empirical covariance functions.

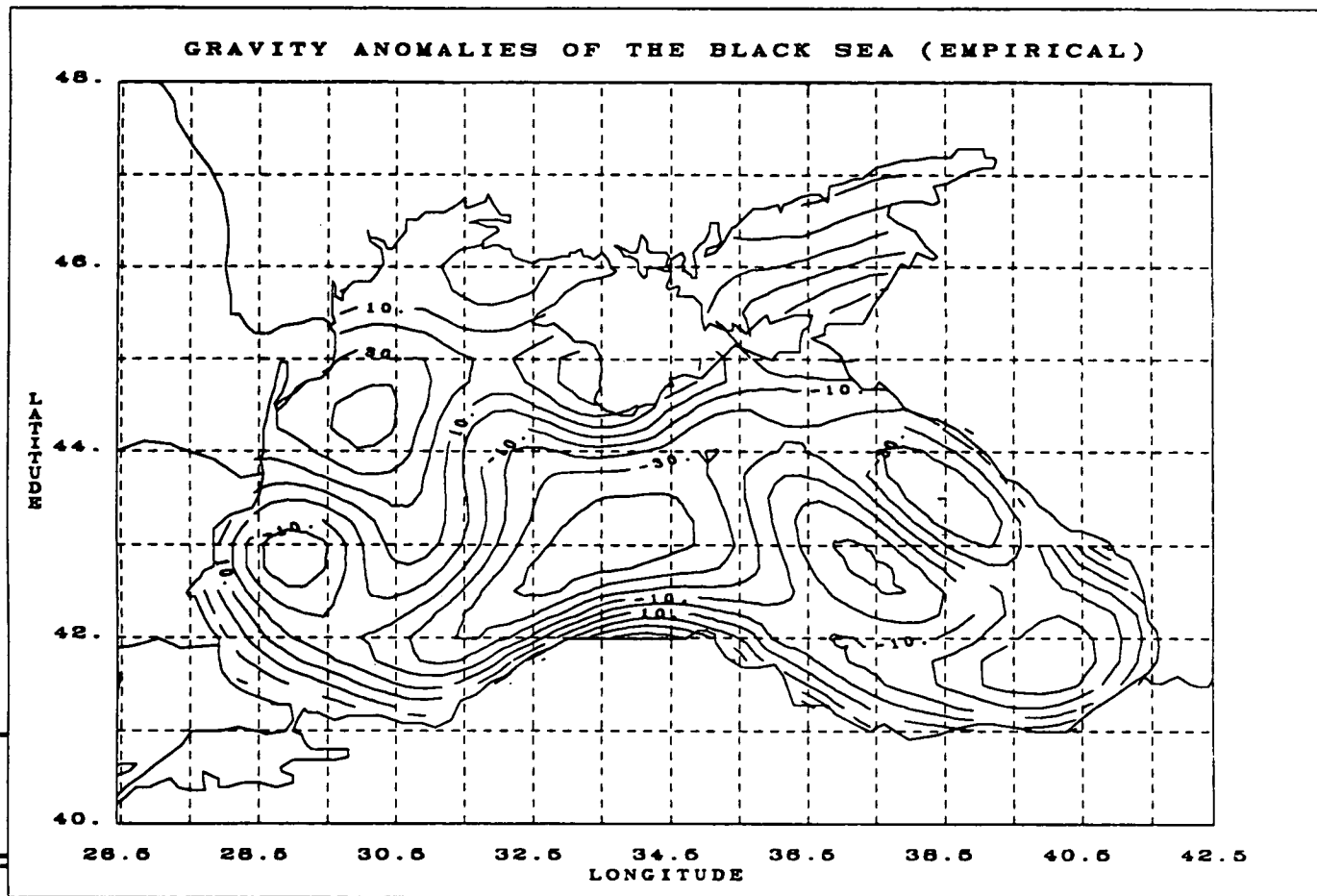


Figure 19. A contour map of estimated gravity anomalies (mgal) of the Black Sea predicted with local empirical covariance functions.

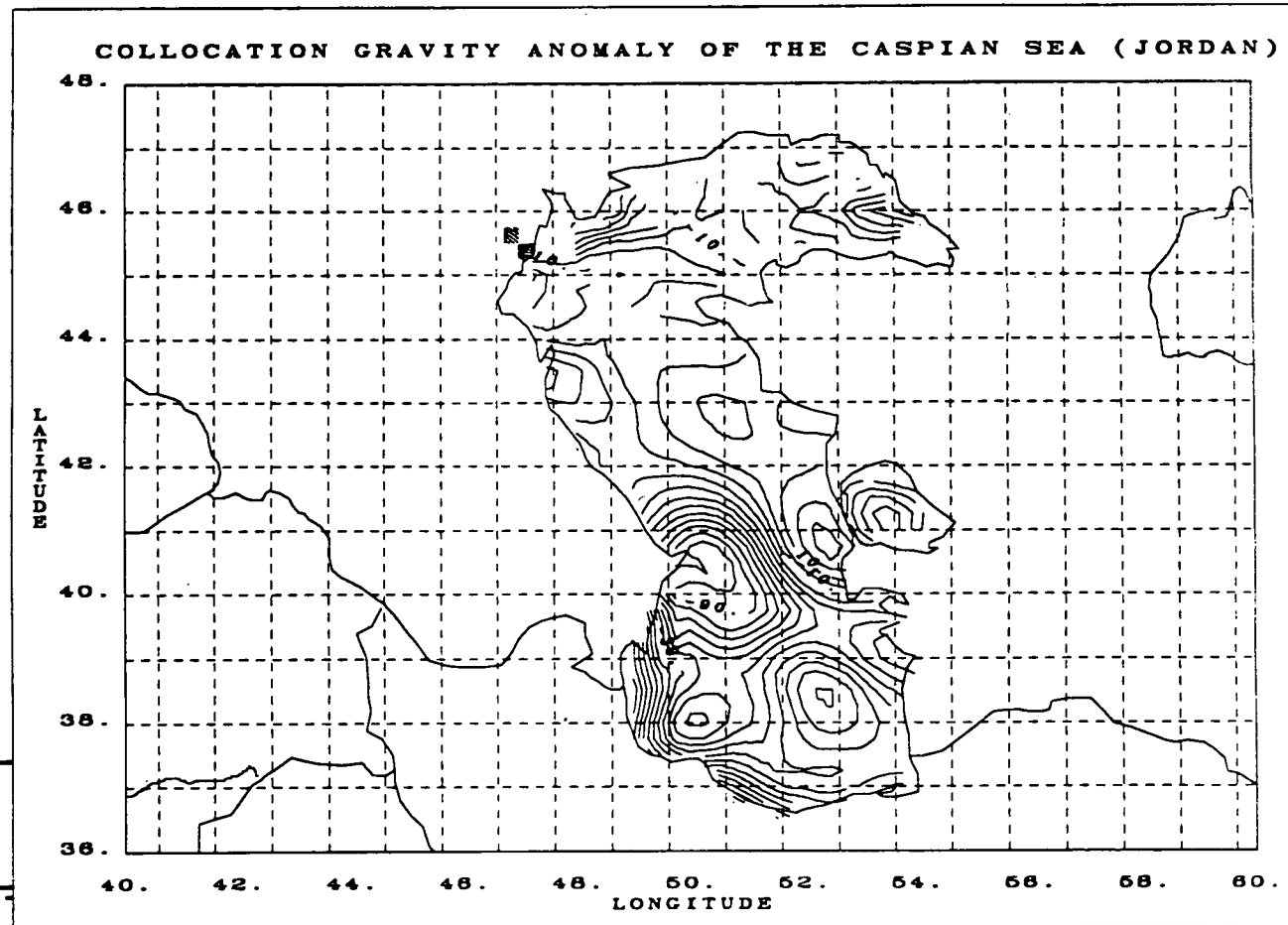
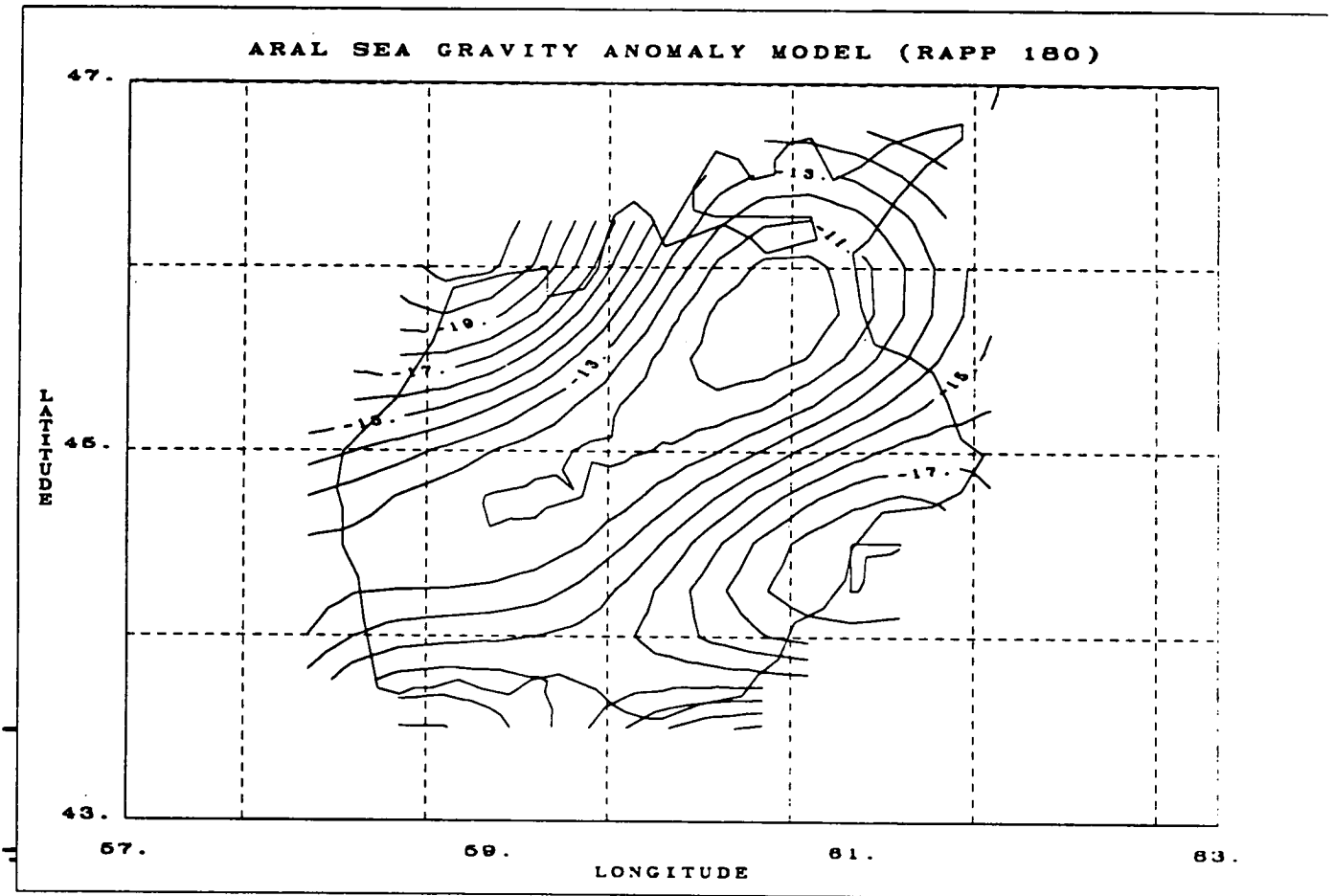


Figure 20. A contour map of estimated gravity anomalies (mgal) of the Caspian Sea predicted with hybrid local empirical covariance functions.

III



III Figure 21. A contour map of Rapp's 180 X 180 reference gravity anomalies (mgal) of the Aral Sea.

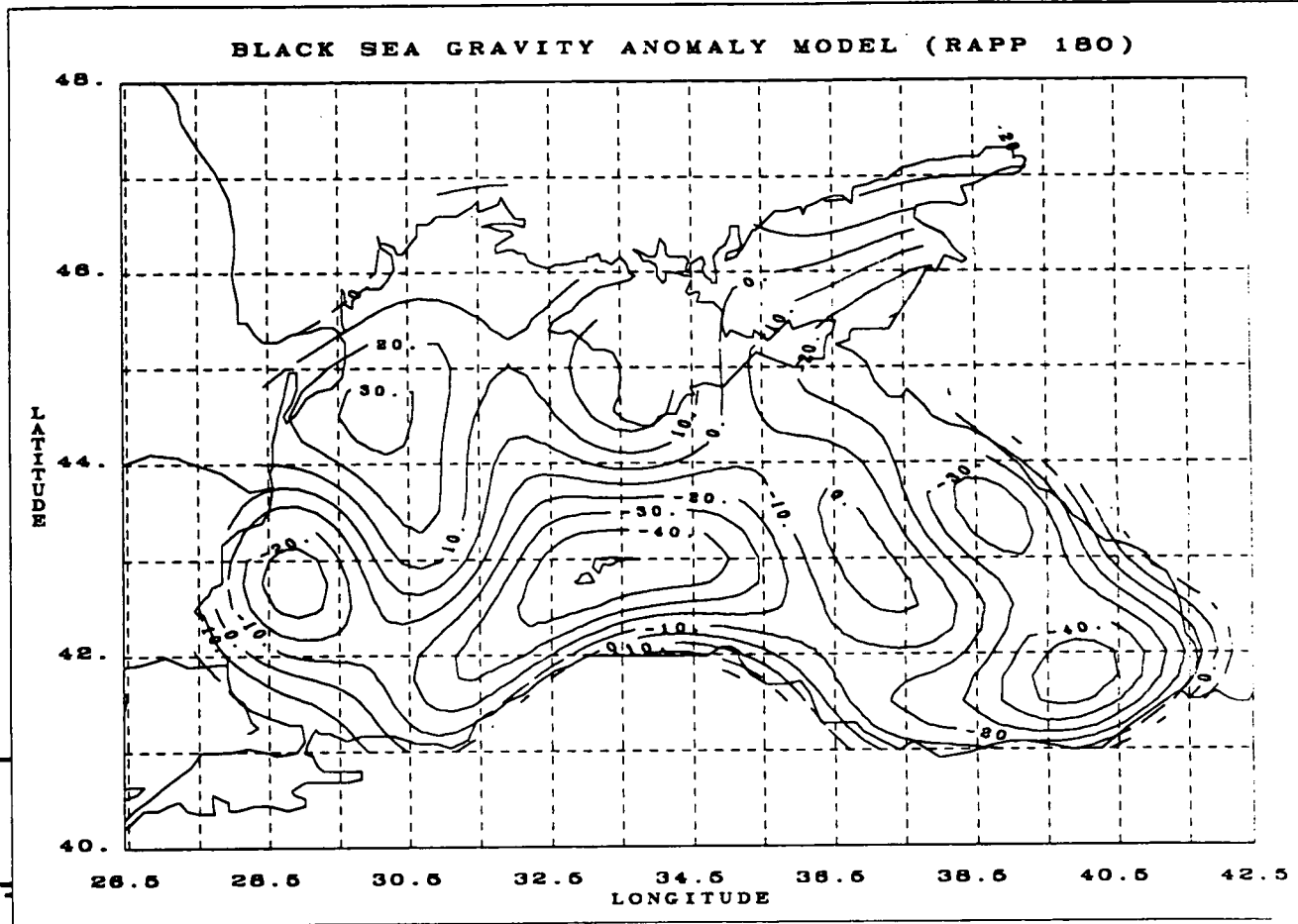
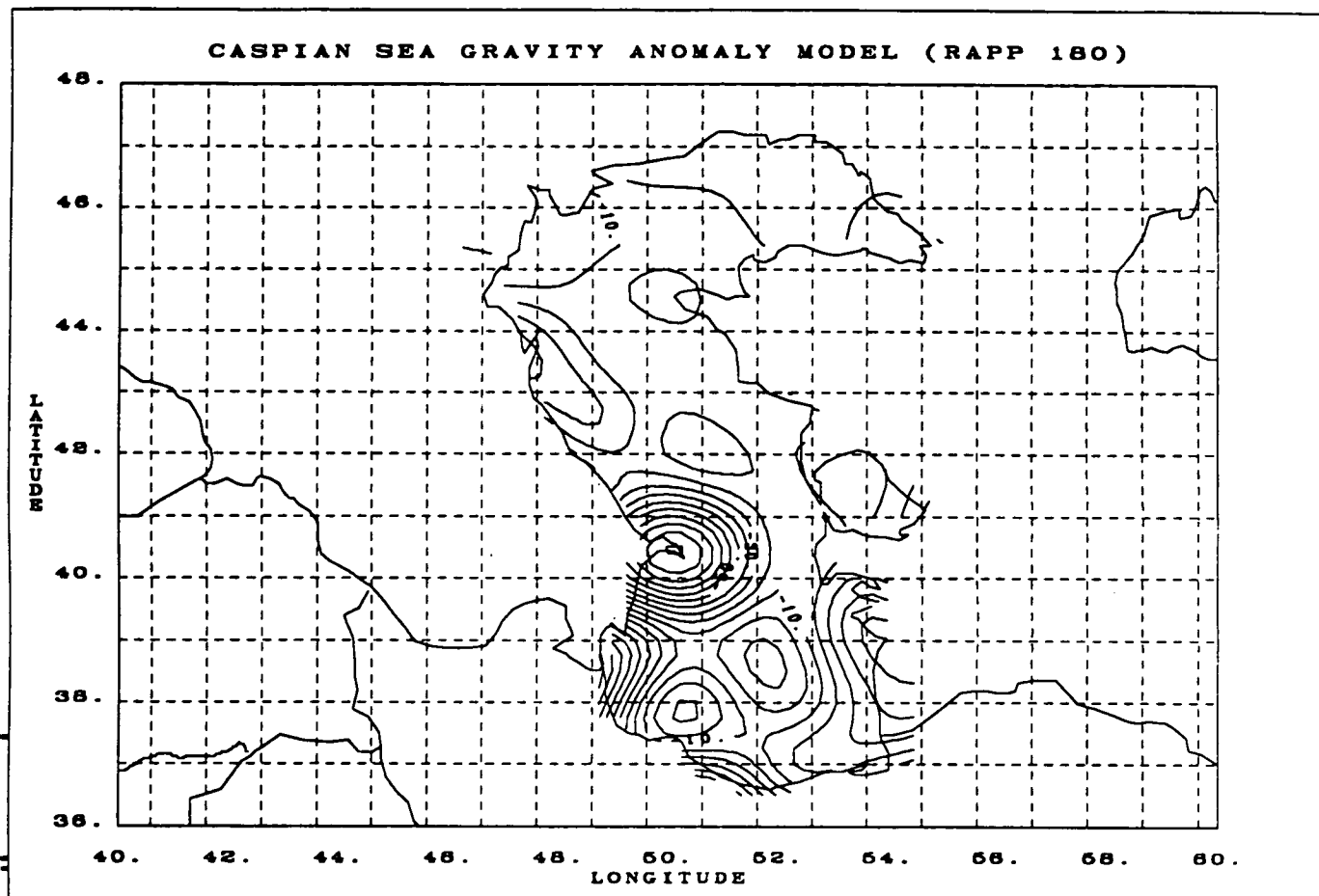


Figure 22. A contour map of Rapp's 180 X 180 reference gravity anomalies (mgal) of the Black Sea.



iii Figure 23. A contour map of Rapp's 180 X 180 reference gravity anomalies (mgal) of the Caspian Sea.



transformation on the information content (or quality) of the reference model. The Black Sea was chosen for this test because of the availability of short-wavelength information in the reference models.

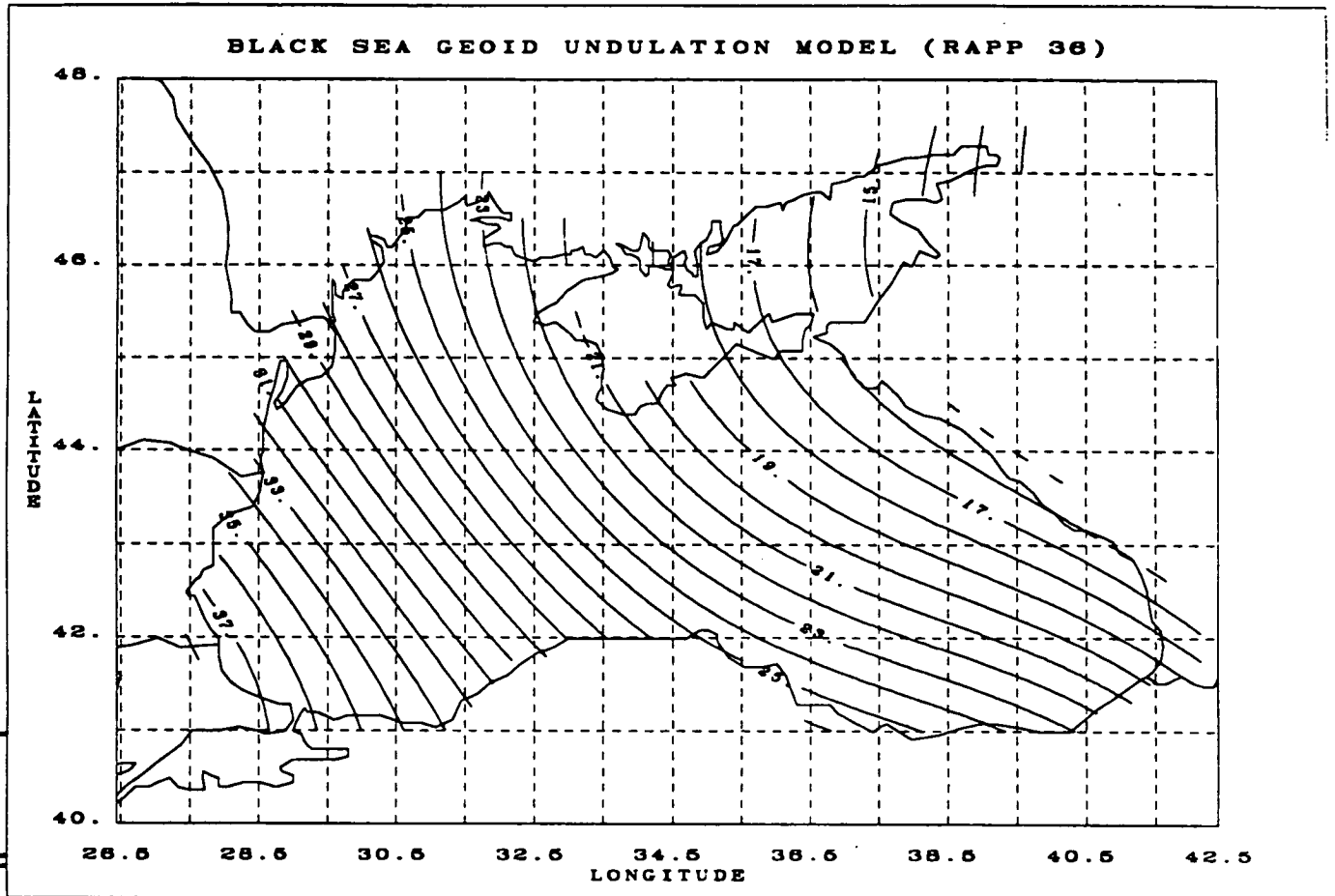
A degraded reference model over the Black Sea is obtained by including only long wavelength (36 X 36) terms of Rapp's 180 X 180 model. Contour maps of the geoid undulations and gravity anomalies from this degraded reference model are shown in Figures 24 and 25, respectively. The geoid-to-gravity transformation is performed using both the degraded reference model and Rapp's 180 X 180 covariance function. The resultant gravity anomalies are shown in Figure 26. It is apparent, comparing with Figure 22, that the quality of the geoid-to-gravity transformation degrades as that of the quality of the reference model. A contour map of the difference between the estimated gravity anomalies using Rapp's 180 X 180 reference model and 36 X 36 reference model is shown in Figure 27. The RMS of the difference is 1.35 mgal, with several broad areas where the difference exceeds 15 mgal.

An iterative transform process to improve performance when using a poorer reference model has also been attempted. To evaluate this algorithm in a controlled test, Rapp's 300 X 300 geopotential model is adopted as the true representation of the geoid and gravity over the Black Sea. The geoid surface derived from the 300 X 300 model provides a grid of input data for the geoid-to-gravity transformation. Both the 180 X 180 and 36 X 36 model are tested as reference surfaces in this benchmark test. The iterative transformation method consists of the following steps:

- a) Use Rapp's covariance function to transform the observed geoid data to gravity anomalies;
- b) Use the same covariance function to transform the calculated gravity anomalies back to geoid heights;
- c) Calculate the RMS difference between the transformed result and the reference model for both the geoid and gravity anomalies;
- d) Use the transformed gravity anomalies and transformed geoid results to form a new set of local residual empirical covariance functions;
- e) Repeat steps a-d using the newly constructed local residual empirical covariance functions for transformation and using the transformed results as new starting reference model, until the RMS difference satisfies a convergence criterion.

It is observed that using the iterative process for both the 180 X 180 and 36 X 36 reference model, a major correction to the reference models occurs during the first and second iterations. The iterative process converges in less than five iterations for reasonable integration cap radius, such as one degree. The transformed gravity anomalies based on 180 X 180 and 36 X 36 reference models are shown in Figures 28 and 29, respectively. Contour maps of the "true" geoid undulations and gravity anomalies according to Rapp's 300 X 300 model are shown in Figures 30 and 31, respectively. The iterative method does improve results when a good (180 X 180) reference surface is used, but does not seem to materially improve the transformation when a poor (36 X 36) reference surface is used.

iii



iii Figure 24. A contour map of Rapp's 36 X 36 reference geoid undulations (m above mean sea level) of the Black Sea.

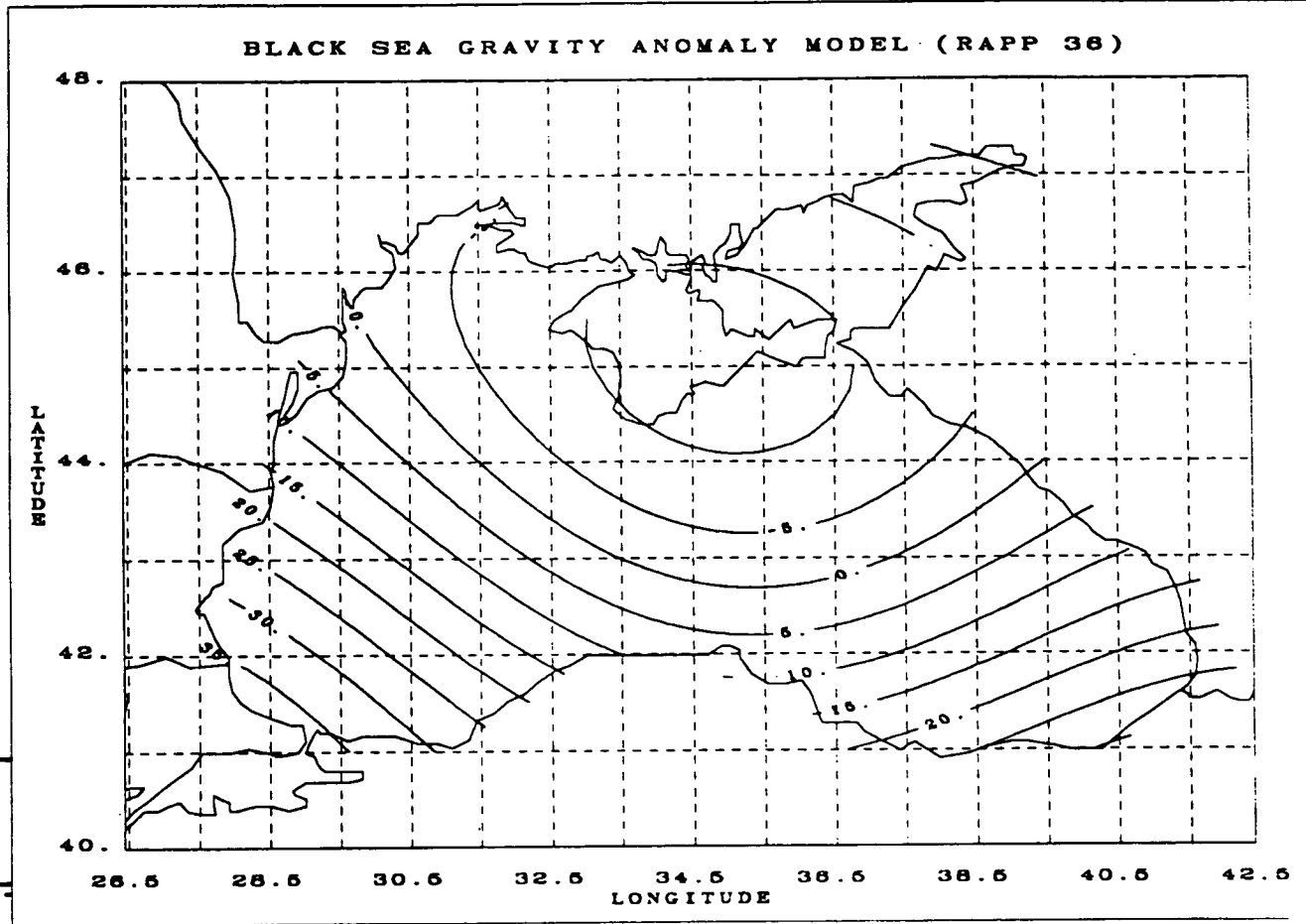
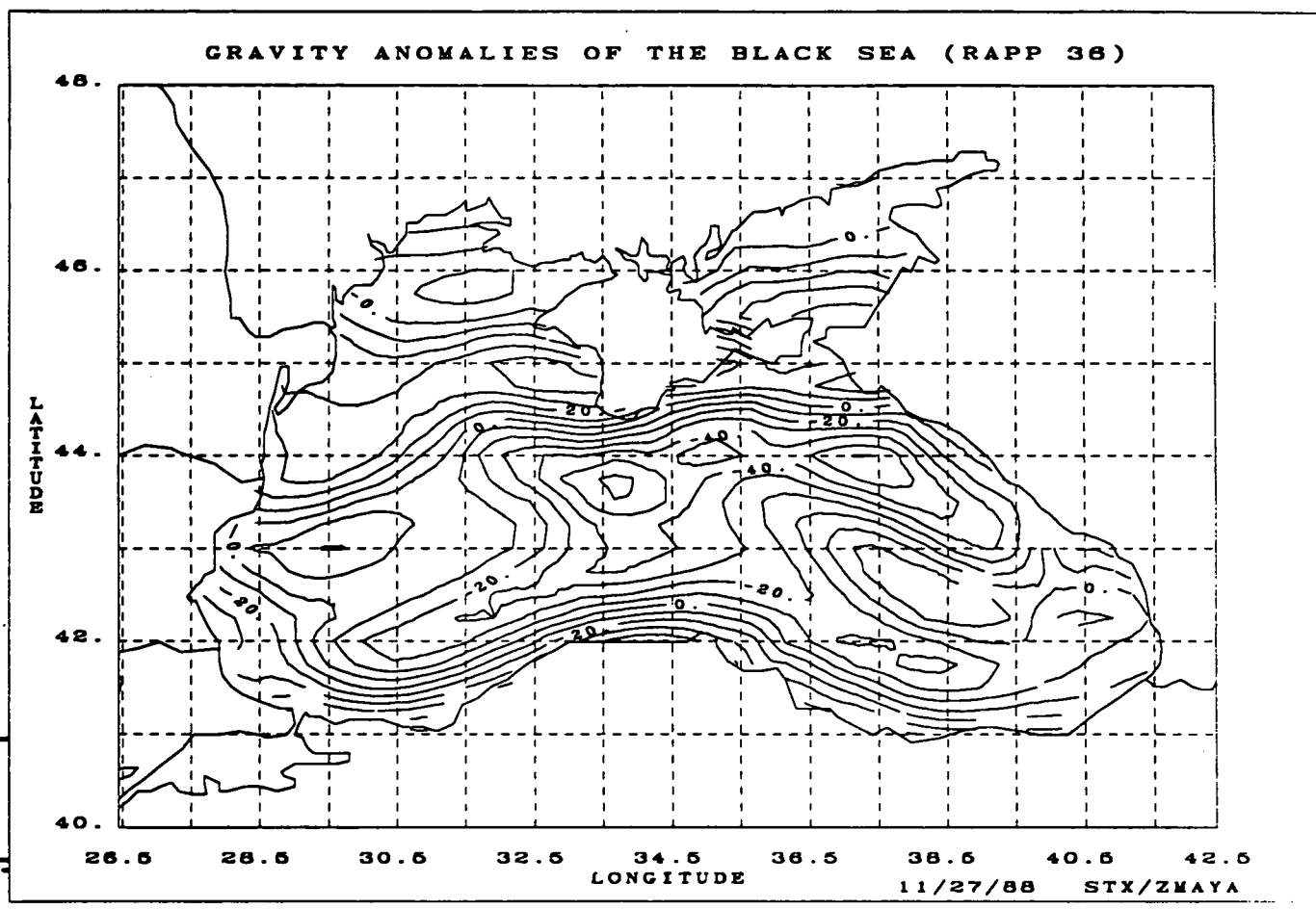


Figure 25. A contour map of Rapp's 36 X 36 reference gravity anomalies (mgal) of the Black Sea.



... Figure 26. A contour map of estimated gravity anomalies (mgal) of the Black Sea based on Rapp's 36 X 36 reference geopotential model.

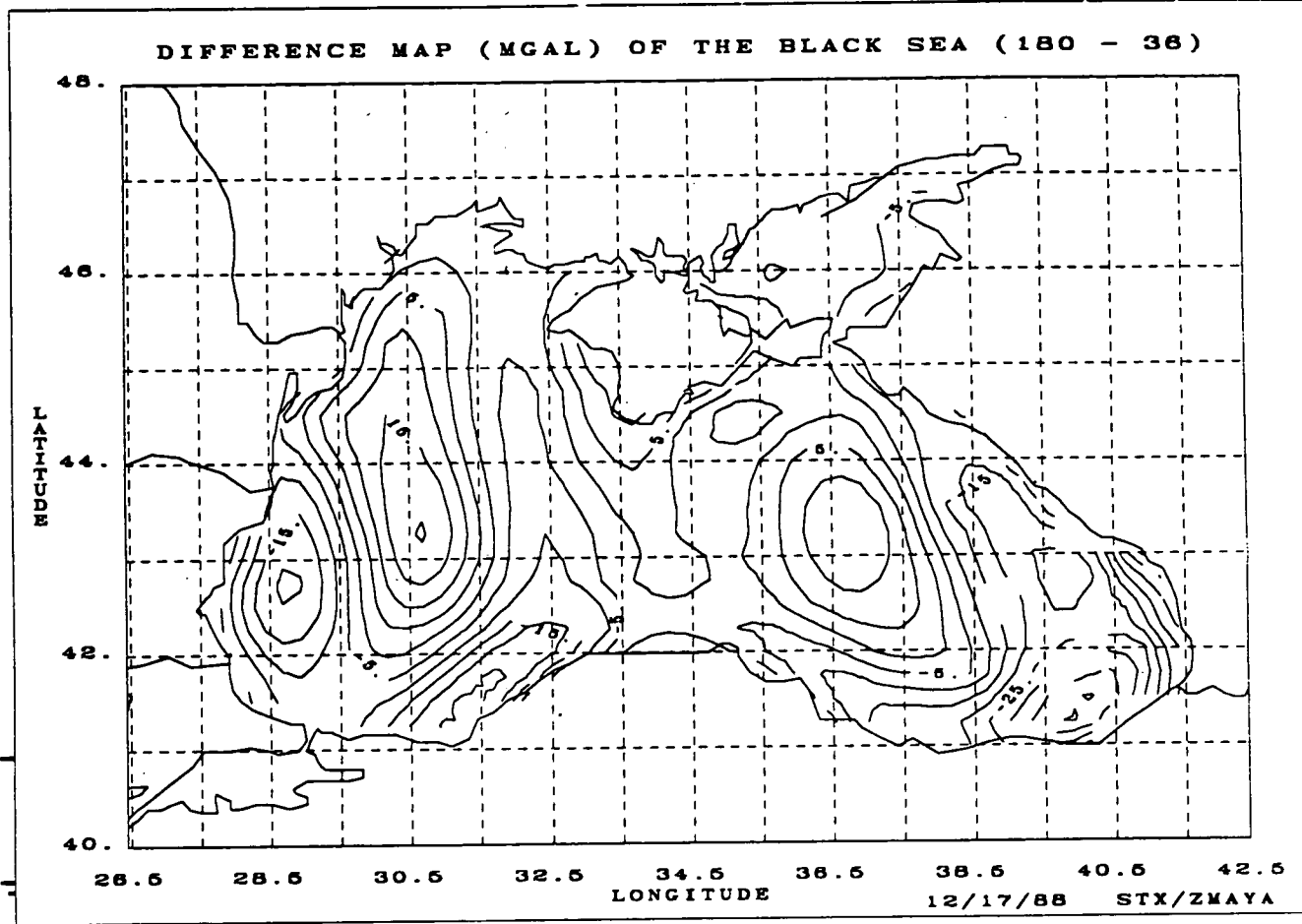


Figure 27. A contour map of the difference between estimated gravity anomalies (mgal) of the Black Sea using Rapp's 36 X 36 and 180 X 180 reference geopotential models.

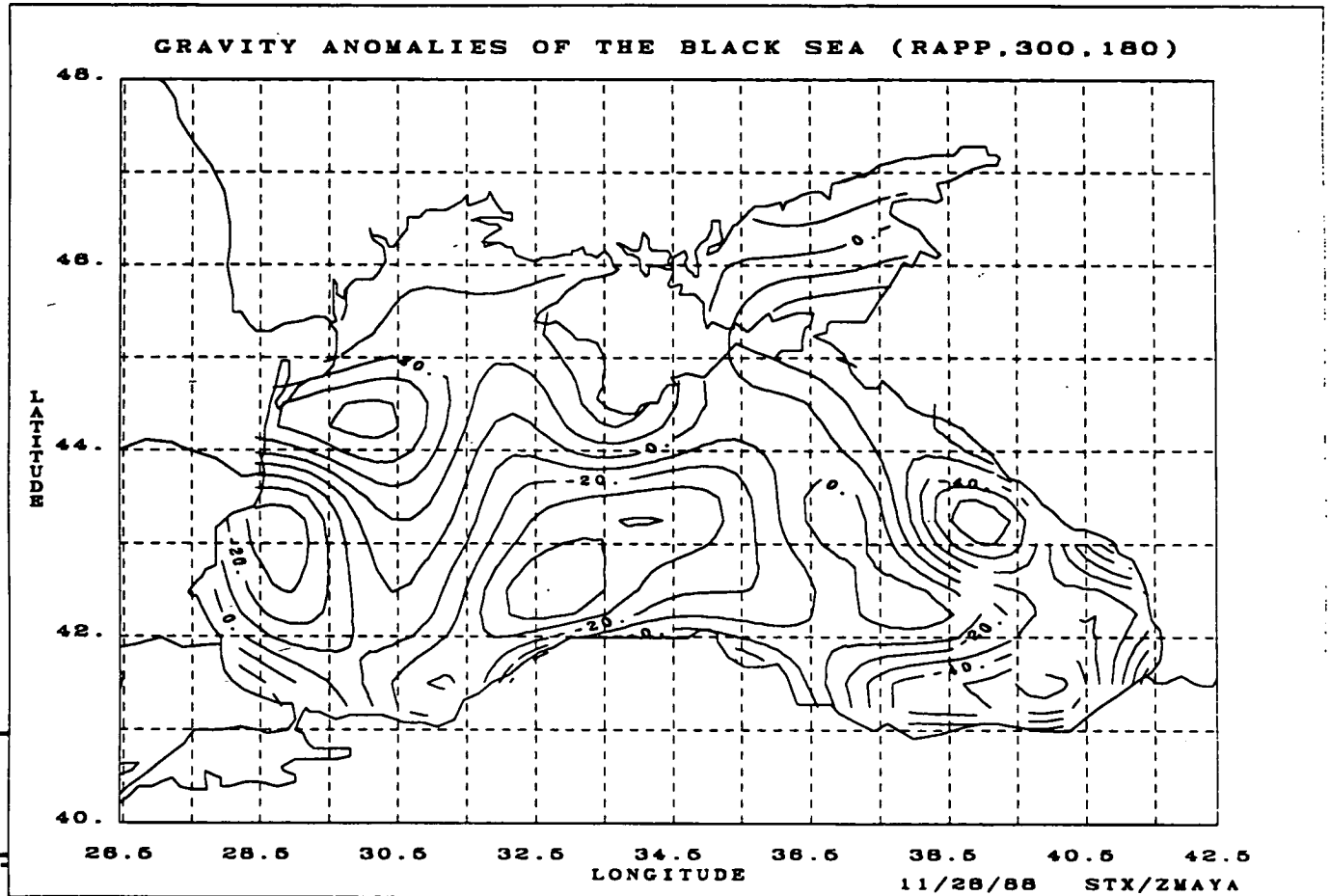


Figure 28. A contour map of estimated gravity anomalies (mgal) of the Black Sea based on Rapp's 180 X 180 reference geopotential model and the self-consistent iterative approach. Rapp's 300 x 300 model geoid undulations are used as input data. This is a test of the iterative approach.

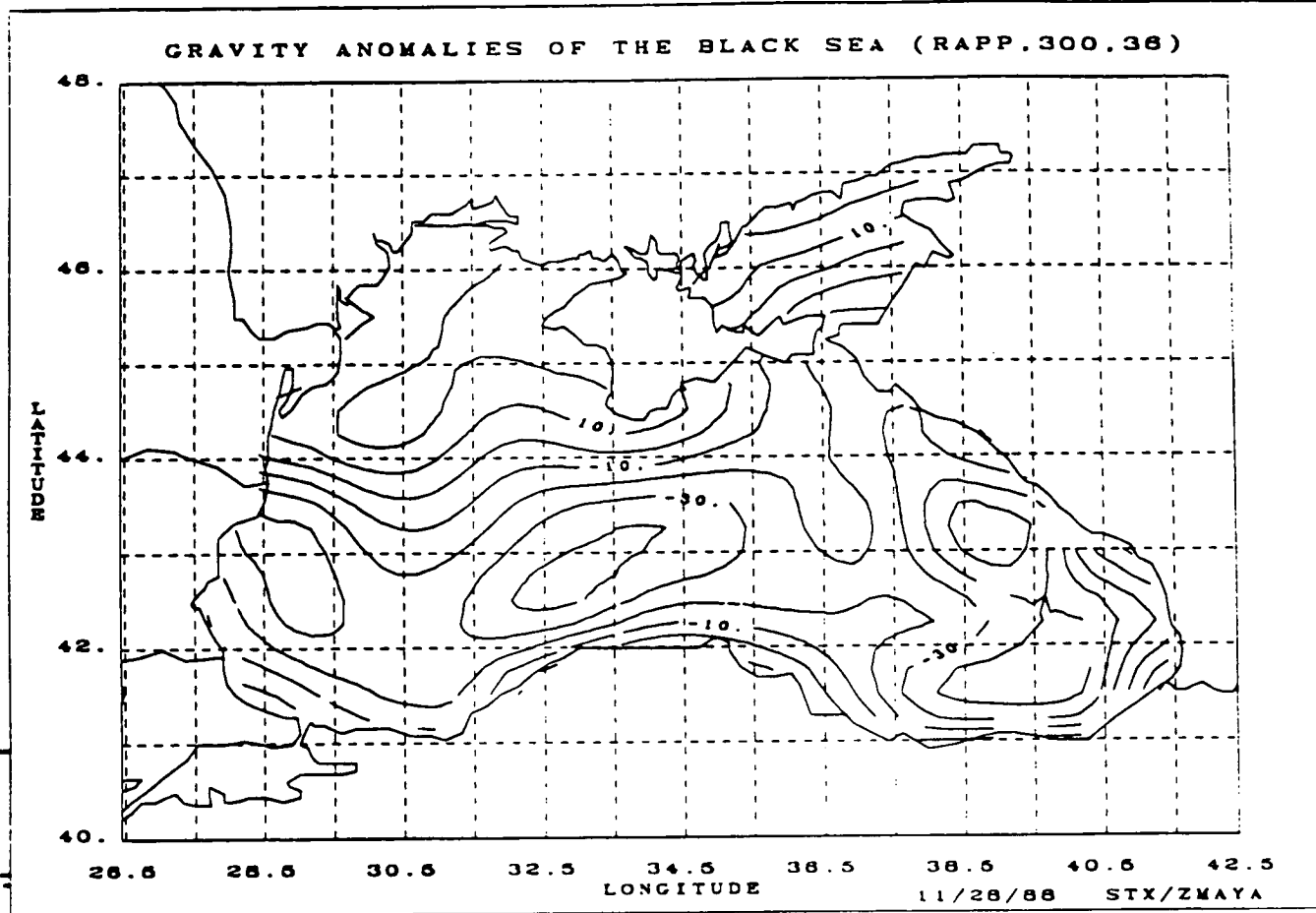


Figure 29. A contour map of estimated gravity anomalies (mgal) of the Black Sea based on Rapp's 36 X 36 reference geopotential model and the self-consistent iterative approach. Rapp's 300 x 300 model geoid undulations are used as input data. This is a test of the iterative approach.

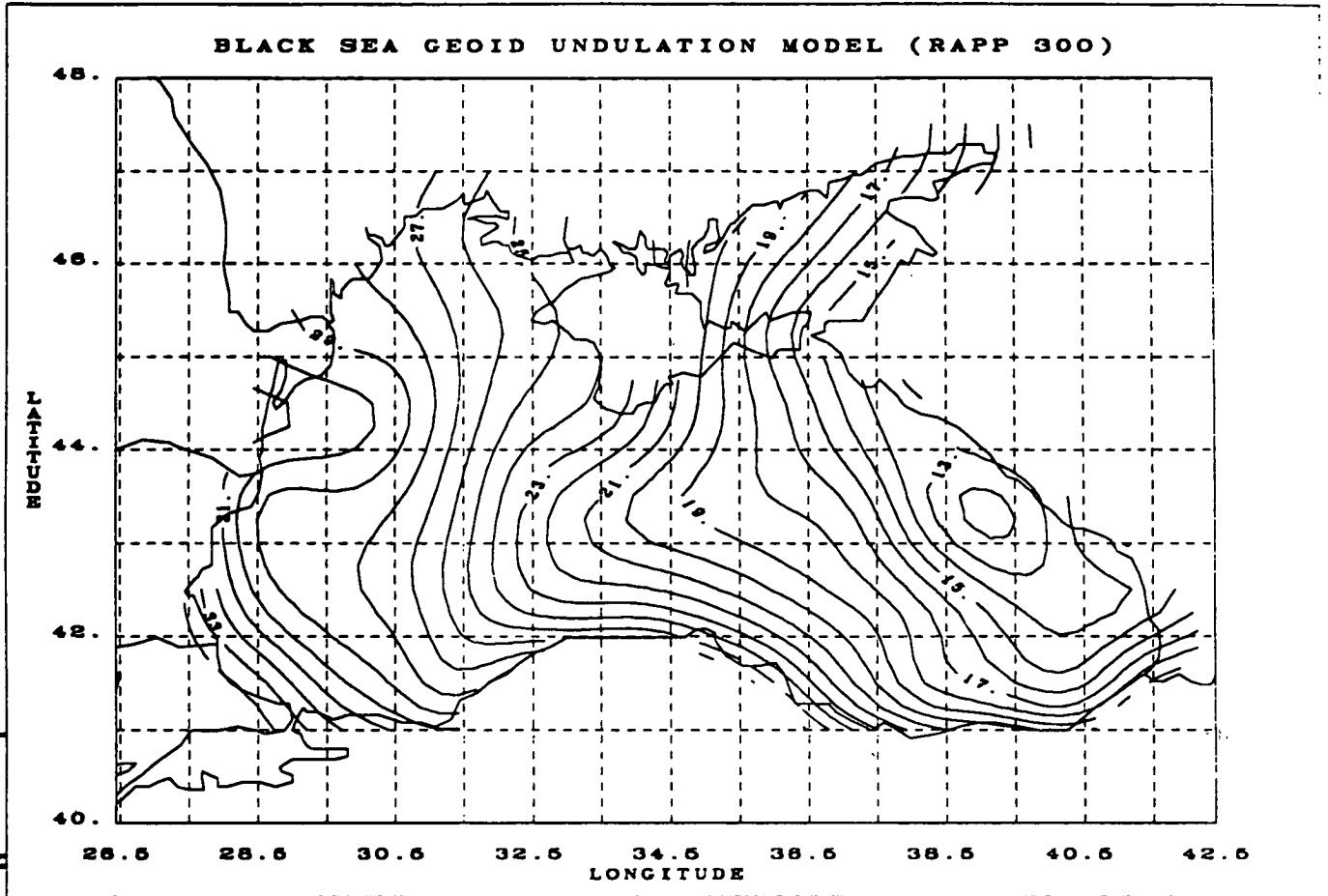
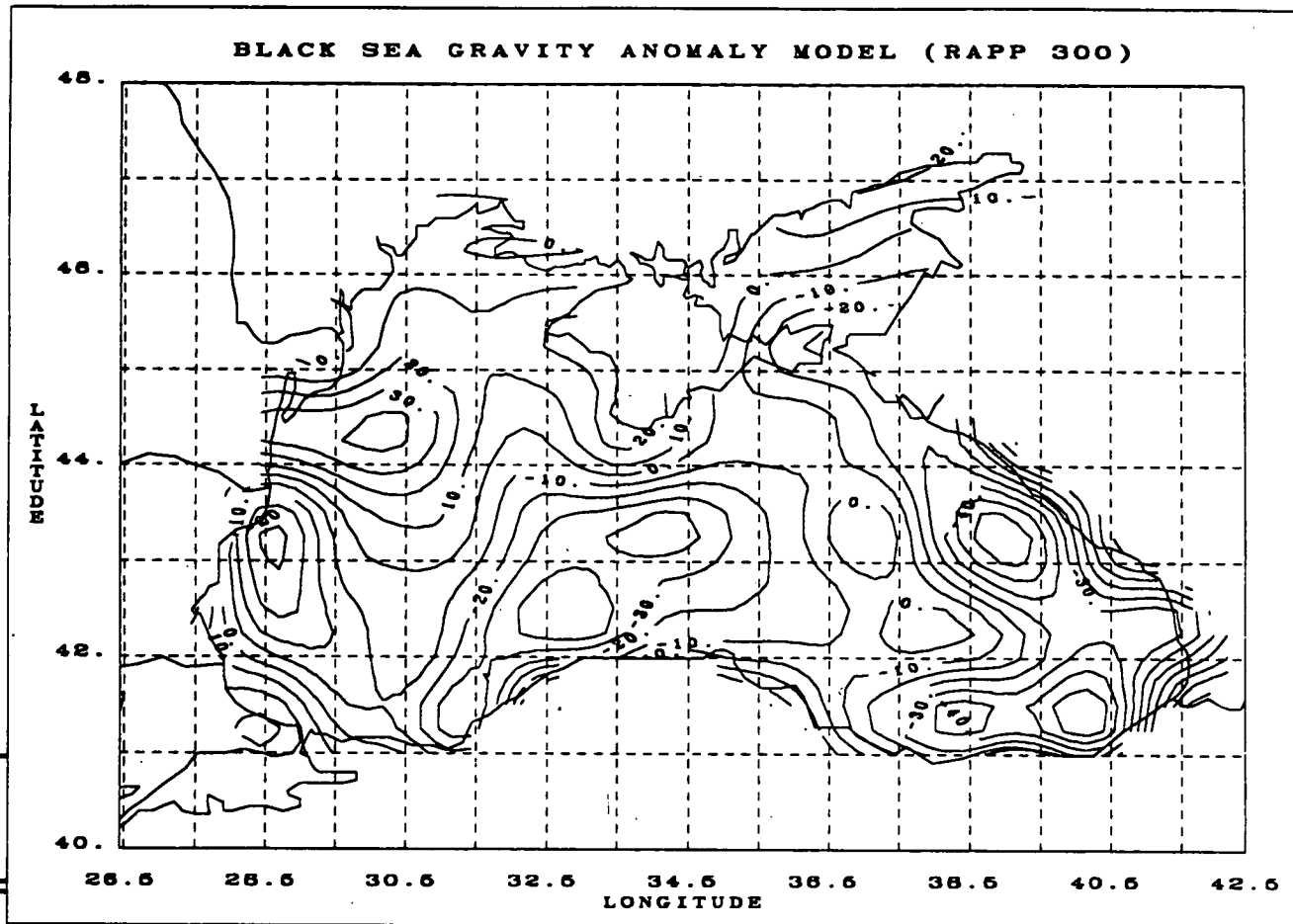


Figure 30. A contour map of Rapp's 300 X 300 reference geoid undulations (m above mean sea level) of the Black Sea.





|| Figure 31. A contour map of Rapp's 300 X 300 reference gravity anomalies (mgal) of the Black Sea.

The sensitivity of the geoid-to-gravity transformation to different covariance functions and information content of the reference models is quantified by determining the RMS of the difference between the "true" gravity anomalies and the estimated ones, as shown in Table 1.

transformation covariance functions	180 X 180 reference model (mgal RMS)	36 X 36 reference model (mgal RMS)
Rapp's	4.47	14.39
Jordan's	4.34	11.12
Iterative	3.19	11.79

Table 1 Error of commission in the geoid-to-gravity transformation as a function of different transformation algorithms using 1° cap size for the integration region. Rapp's 180 X 180 and 36 X 36 models are used as reference surfaces.

The RMS values represent the error of commission in the geoid-to-gravity transformation. In order to stabilize the covariance matrix, an *a-priori* noise must be added. To make the comparison fair, a common *a-priori* stabilizing variance of  $(25 \text{ cm})^2$  was added for all three covariance functions when the 180 X 180 reference field was used, and  $(60 \text{ cm})^2$  was added whenever the 36 X 36 reference field was used. The iterative algorithm based on empirical covariance functions, compared to the single-pass transformation based on Rapp's and Jordan's covariance functions, generally yields the best recovered gravity anomalies when the information spectra limit of the reference model is commensurate with the cap size (180 X 180 model and 1° cap size).

When the stabilizing *a-priori* error variances are removed or reduced to lower values, while still maintaining solution stability, the RMS error of commission is generally reduced, along with the formal prediction error. For example, in the case of Jordan's covariance function, when the *a-priori* variance is reduced to  $(10 \text{ cm})^2$ , the corresponding values in Table 1 become 2.97 mgal and 6.96 mgal respectively for 180 X 180 and 36 X 36 reference models. In fact, these levels of stabilizing noise seem to be optimal for both the Jordan and Rapp covariance functions, because lower and higher values of *a-priori* noise result in larger RMS errors of commission. The error of commission for Rapp's covariance function is universally a few percent higher than that for Jordan's covariance function. On the other hand,  $(60 \text{ cm})^2$  is optimal (and necessary) for the empirical local covariance function. Based on these results, we conclude that Jordan's covariance function is best for gravity prediction in the Black Sea region, and that the optimal level of *a-priori* noise is about 10 cm. Furthermore, we conclude that the error of commission of the least squares collocation technique for gravity prediction is highly dependent on the quality of the reference model and ranges from 3 to 7 mgal.

It should be appreciated that collocation is a statistical method that relies on the transformation covariance functions to provide the physics of the figure of the Earth and

its gravity field. The iterative algorithm is a hybrid of a perturbation on the reference surface and an information shaping/filtering process. The initial shaping filter, the covariance function, should conform with the information content of the initial reference surface. That is, for a reference model whose short wavelength cutoff is at  $1^\circ$ , the covariance function should represent information of wavelengths shorter than  $1^\circ$  and the integration cap size should have a commensurate size. It is speculated that when the  $36 \times 36$  model is used as reference surface, long-wavelength correction to the updated reference surface is limited to wavelengths less than one degree because of the chosen integration cap size of one degree. Wavelength components longer than one degree and less than 5 degrees, therefore, must be corrected in order to improve the  $36 \times 36$  reference model. The integration cap size, then, should be commensurate with its shortest wavelength of the reference model. A large integration cap size, unfortunately, will result in forbiddingly high computing cost unless the data grid for the initial iterative steps is decimated. The cap size can be gradually reduced, as the data density is gradually increased, in subsequent iterations. However, an algorithm developed to maintain constant density of data in each iterative step, performed worse.

Further effort in the attempt of improving the geoid-to-gravity transformation algorithm includes the use of local empirical anisotropic covariance functions. A preliminary progress report in this attempt is given in Brown *et al.* (1990).

## V. GEOPHYSICAL INFERENCES

The inland sea region have undergone different episodes of orogeny. The gravity anomalies characteristic of this region should bear the signatures of the past tectonic activities. Before our predicted gravity results are integrated into the regional data base, a reference regional gravity-anomaly map will first be reviewed.

A reference map of the gravity anomalies over the inland sea region derived from Rapp's  $180 \times 180$  geopotential model is shown in Plate 1. The same regional map but with the predicted gravity results for the inland seas superimposed on it is shown in Plate 2. More detailed features over the inland seas can be delineated based on the predicted results because the predicted results are derived from high-resolution altimetric geoid data. There are three areas where the predicted results deviate significantly from the reference map. According to the reference model, the signature of the anomalies are generally negative east of the Crimea and in the northern part of the Caspian Sea. At the southern Caspian Sea, there seems to be a break in a broad region of negative anomalies. Over the Aral Sea, the signature of the predicted gravity anomalies is generally negative. According to the predicted results (see Plate 2), there is a band of positive anomalies east of Crimea instead of a general low as shown in the reference map (Plate 1). At the southern Caspian Sea, two aforementioned regions of negative anomalies are connected. There is also a broad band of positive anomalies instead of general region of negative anomalies at the northern part of the Caspian Sea. The signature of gravity anomalies changed from negative to positive in the eastern and southern portion of the Aral Sea. There is, therefore, a continuous region of positive gravity anomalies extending from the

northern part of the Caspian Sea, across the Ust-Yurt Plateau, to the Kyzyl Kum. Aside from these differences, the general features of the predicted results and the reference model are quite compatible.

It has been speculated that there is a continuous suture running from the Crimea, along the spine of the Greater Caucasus, through the Aspheron peninsula, across the southern Caspian, and into the Kopet mountains (Sengör, 1984). Our current data seems to be compatible with such a conjecture. In the north, there is a band of positive anomalies in alignment with the Dnieper-Donetsk aulacogen and the South Mangyshlak-Ust-Yurt ridge and basin. This coincidence suggests that the Dnieper-Donetsk aulacogen and the South Mangyshlak-Ust-Yurt ridge may be of a common origin. It has also been suggested that there is a Tethyan geosyncline tracing southward, running across the northern reach of the Black Sea, into the northern part of the Caspian Sea, and then going northward.

Aside from these prominent features, the west Black Sea depression can also be identified by the signature of the negative anomalies. However, the predicted anomalies is positive over the east Black Sea depression. The Arkhangelsky Swell is coincident with area of positive anomalies. Contrary to expectations, the Andrusov Swell and the Shatsky Swell are coincident with areas of negative anomalies. This peculiar behavior in the signature of gravity anomalies may be due to crustal flexure, because of the compressional forces resulting from the northward movement of the Arabian promontory. The gravity high over the east Black Sea depression may be a consequence of compressional forces. Uncompensated sediment deposits at river deltas also show up as positive gravity anomalies, such as the case for the Danube, the Volga, the Ural, the Syr-Dar'ya and the Amu-Dar'ya.

## REFERENCES

- Au, A.Y., R.D. Brown and J.E. Welker, 1989a, *Analysts of Altimetry Over Inland Seas*, **NASA Technical Memorandum 100729**, Washington, DC.
- Au, A.Y., R.D. Brown and J.E. Welker, 1989b, *Programs for Processing Altimeter Data Over Inland Seas*, **NASA Technical Memorandum 100730**, Washington, DC.
- Au, A.Y., R.D. Brown and J.E. Welker, 1990, *Analysts of Altimetry Over the Aral Sea*, **NASA Technical Memorandum 100759**, Washington, DC.
- Brown, R.D., A.Y. Au and J.E. Welker, 1990, "Anisotropic covariance functions for local gravity prediction, *Eos Trans. AGU*, **70**, p. 303.
- Cheney, R.E., L. Miller, R.W. Agreen, N.S. Doyle and B. Douglas, 1989, *Monitoring Tropical Sea Level in Near-Real Time with GEOSAT Altimetry*, Johns Hopkins APL Tech. Dig. **10**, pp. 362-368.
- Cowley, J.M. and A.Y. Au, 1978, "Diffraction by crystals with planar faults. III: Structure analysis using microtwins", *Acta Crystallogr.*, **B34**, pp. 739-743.
- Jordan, S.K., 1972, "Self-constant statistical models for gravity anomaly, vertical deflections, and undulation of the geoid", *J. Geophys. Res.*, **77**, pp. 3660-3670.
- Knudsen, P., 1987, "Estimation and modelling of the local empirical covariance function using gravity and satellite altimeter data", *Bull. Geod.*, **61**, pp. 145-160.
- Knudsen, P., 1988, *Determination of Local Empirical Covariance Functions from Residual Terrain Reduced Altimeter Data*, Reports of the Department of Geodetic Science and Surveying, **No. 395**, Ohio State University, Columbus, OH.
- Mazzega, P. and S. Houry, 1989, "An experiment to invert SEASAT altimetry for the Mediterranean and Black Sea mean surfaces", *Geophys. Jour.*, **96**, pp. 259-272.
- Moritz, H., 1978, "Least-squares collocation", *Rev. Geophys. Space Phys.*, **16**, pp. 421-430.
- Sengör, A.M.C., 1984, *The Cimmeric Orogenic System and the Tectonics of Eurasia*. *Geol. Soc. Amer.*, **Special Paper 195**.
- Stanley, H.R., 1979, "The Geos 3 Project" *J. Geophys. Res.*, **84**, pp. 3779-3783.
- Rapp, R.H., 1986, "Gravity anomalies and sea surface heights derived from a combined GEO-3/SEASAT altimeter data set", *J. Geophys. Res.*, **91**, pp. 4867-4876.

Townsend, W.F., 1980, "An initial assessment of the performance achieved by the SEASAT radar altimeter", *IEEE J. Oceanic Eng.*, **OE-5**, pp. 80-92.

Treitel, S. and E.A. Robinson, 1966, "The design of high-resolution digital filters", *IEEE Trans. on Geoscience electronics*, **GE-4**, pp. 25-38.

Wagner, C.A., 1979, "The geoid spectrum from altimetry", *J. Geophys. Res.*, **84**, pp. 3861-3871.

INLAND SEAS GRAVITY ANOMALIES (RAPP'S MODEL)

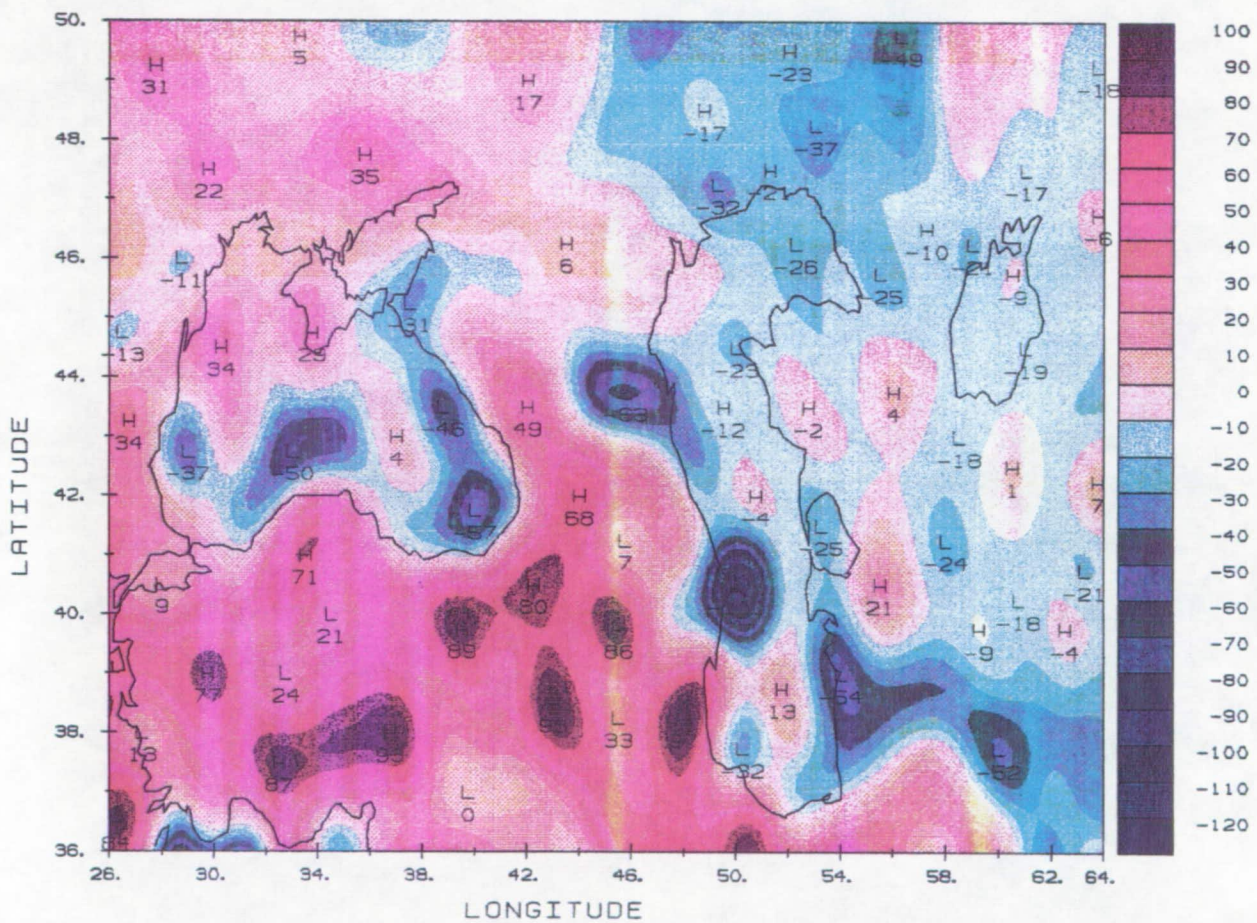


Plate 1. A contour map of Rapp's 180 X 180 reference gravity anomalies (mgal) of the inland seas region.

## INLAND SEAS GRAVITY ANOMALIES

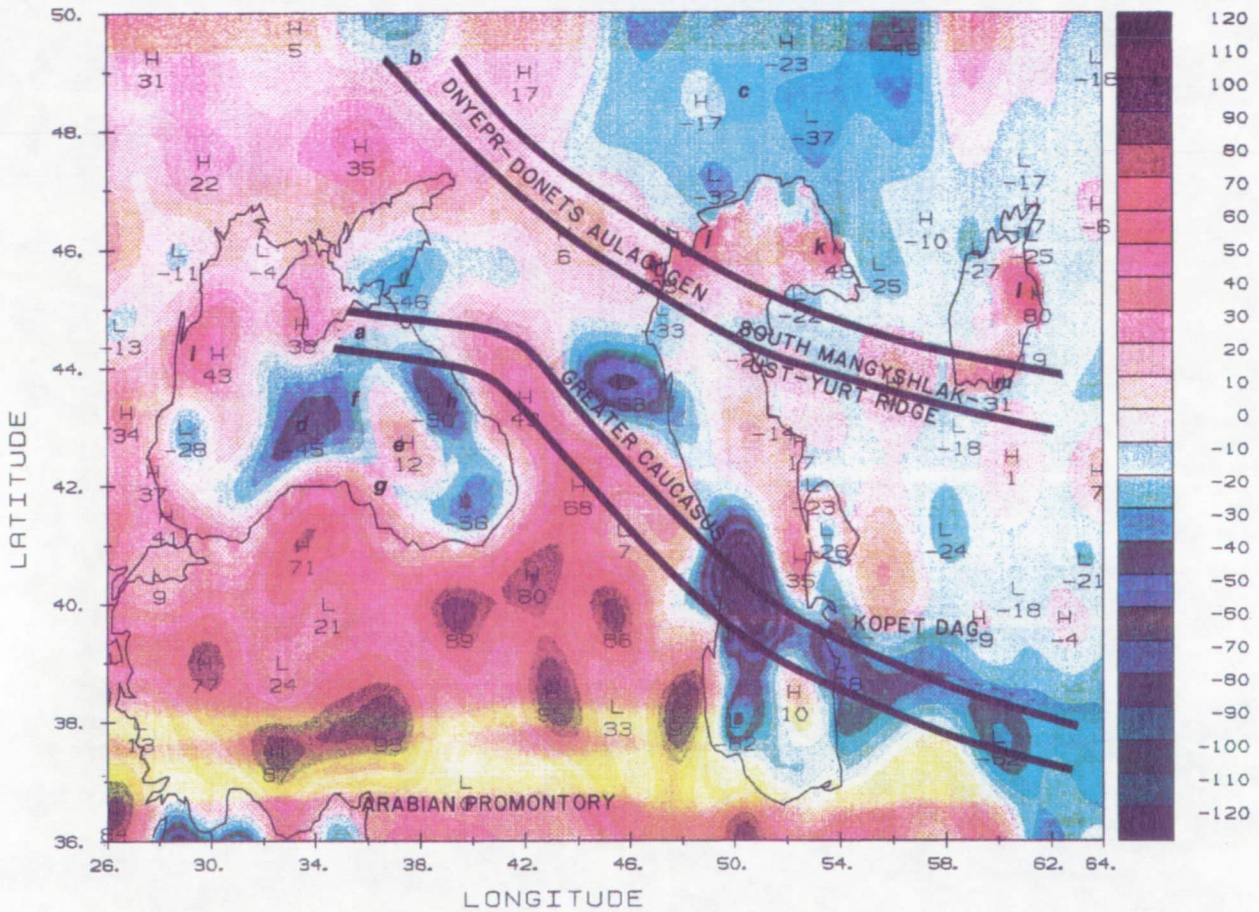


Plate 2. A contour map of predicted gravity anomalies (mgal) of the inland seas region. (a) Continuous suture running from the Crimea, along the spine of the Greater Caucasus, through the Aspheron peninsula, across the southern Caspian, and into the Kopet mountains; (b) Band of positive anomalies in alignment with the Dnieper-Donetsk aulacogen and the South Mangyshlak-Ust-Yurt ridge and basin; (c) Tethyan geosyncline tracing southward, running across the northern reach of the Black Sea, into the northern part of the Caspian Sea, and then going northward; (d) The west Black Sea depression; (e) The east Black Sea depression; (f) The Andrusov Swell; (g) The Arkhangelsky Swell; (h) The Shatsky Swell; (i) The Danube delta; (j) The Volga delta; (k) The Ural delta; (l) The Syr-Dar'ya delta and (m) The Amu-Dar'ya delta.



## Report Documentation Page

<b>1. Report No.</b> NASA TM 104543	<b>2. Government Accession No.</b>	<b>3. Recipient's Catalog No.</b>	
<b>4. Title and Subtitle</b> Geoid Undulations and Gravity Anomalies Over the Aral Sea, the Black Sea and the Caspian Sea From a Combined GEOS-3/SEASAT/GEOSAT Altimeter Data Set		<b>5. Report Date</b> July 1991	
		<b>6. Performing Organization Code</b> 921.0	
<b>7. Author(s)</b> Andrew Y. Au, Richard D. Brown and Jean E. Welker		<b>8. Performing Organization Report No.</b> 91E02481	
		<b>10. Work Unit No.</b>	
<b>9. Performing Organization Name and Address</b> Goddard Space Flight Center Greenbelt, Maryland 20771		<b>11. Contract or Grant No.</b>	
		<b>13. Type of Report and Period Covered</b> Technical Memorandum	
<b>12. Sponsoring Agency Name and Address</b> National Aeronautics and Space Administration Washington, D.C. 20546-0001		<b>14. Sponsoring Agency Code</b>	
		<b>15. Supplementary Notes</b> Andrew Y. Au and Richard D. Brown: ST Systems Corporation, Lanham, Maryland, 20705. Jean E. Welker: Geodynamics Branch, NASA-GSFC, Greenbelt, Maryland, 20771.	
<b>16. Abstract</b> <p>Satellite-based altimetric data taken by GEOS-3, SEASAT and GEOSAT over the Aral Sea, the Black Sea and the Caspian Sea are analyzed and a least-squares collocation technique is used to predict the geoid undulations on a 0.25° x 0.25° grid and to transform these geoid undulations to free air gravity anomalies. Rapp's 180 x 180 geopotential model is used as the reference surface for the collocation procedure. The result of geoid-to-gravity transformation is, however, sensitive to the information content of the reference geopotential model used. For example, considerable detailed surface gravity data have been incorporated into the reference model over the Black Sea, resulting in a reference model with significant information content at short wavelengths. Thus, estimation of short-wavelength gravity anomalies from gridded geoid heights is generally reliable over regions such as the Black Sea, using the conventional collocation technique with local empirical covariance functions. Over regions such as the Caspian Sea, where detailed surface data are generally not incorporated into the reference model, unconventional techniques are needed to obtain reliable gravity anomalies. Based on the predicted gravity anomalies over these inland seas, speculative tectonic structures are identified and geophysical processes are inferred.</p>			
<b>17. Key Words (Suggested by Author(s))</b> altimetry, inland seas, geoid, gravity anomalies, Black and Caspian Seas		<b>18. Distribution Statement</b> Unclassified - Unlimited  Subject Category 46	
<b>19. Security Classif. (of this report)</b> Unclassified	<b>20. Security Classif. (of this page)</b> Unclassified	<b>21. No. of pages</b> 58	<b>22. Price</b>